TECHNICAL REPORT

ON THE COMPUTATION OF BAROTROPIC TIDES IN DEEP ESTUARIES With Application To Knight Inlet, British Columbia

Bruno M. Jamart

WSG 80-6
October 1980

TECHNICAL REPORT

ON THE COMPUTATION OF BAROTROPIC TIDES IN DEEP ESTUARIES With Application To Knight Inlet, British Columbia

Bruno M. Jamart

WSG 80-6
October 1980

Washington Sea Grant Program
Division of Marine Resources
University of Washington HG-30
Seattle, Washington 98105

ACKNOWLEDGMENTS

This research was supported in part by the Washington Sea Grant Program, under grant NA79AA-D-00054, and in part by the Oceanography Section, National Science Foundation, under grant OCE76-00406. The computing facilities at the National Center for Atmospheric Research, sponsored by the National Science foundation, were made available under Project 35371006.

The material contained in this report constitutes part of the thesis I submitted in partial fulfillment of the requirements for the degree of Doctor of Philosophy at the University of Washington. I am grateful to Professors D. F. Winter and C. E. Pearson for their continuous support of this study. It is also a pleasure to acknowledge the artwork of Joyce Lehner Fournier.

Bruno M. Jamart
October, 1980

ABOUT THE AUTHOR

Bruno M. Jamart received his Ph.D. from the University of Washington, Department of Oceanography. He is presently employed at the University of California at Santa Barbara, Department of Mechanical and Environmental Engineering.

KEY WORDS

1. Tidal motion 2. Barotropic tides -- computation 3. Knight Inlet, British Columbia -- tides 4. Finite element method -- tidal model, 5. Spectral method -- tidal computation

Support for publication of this manuscript was provided by Grant No. NA79AA-D-00054 from the National Oceanic and Atmospheric Administration to the Washington Sea Grant Program.

Additional copies of this publication may be obtained from Washington Sea Grant Communications, Division of Marine Resources, University of Washington, HG-30, Seattle, WA 98195.

WSG 80-6
October 1980
Price: $3.50

CONTENTS

ABSTRACT

Tidal motion in semi-enclosed basins is essentially periodic. Hence, the solution of the shallow water wave equations in Fourier space (or in terms of harmonic constituents) can be an efficient alternative to the conventional time-stepping procedures. A numerical method based on that premise is described; the method combines variational calculus, an iterative scheme, and the finite element method to determine the spatial variations of the Fourier coefficients of water height and depth-averaged horizontal velocities. The elimination of the velocities from the continuity equation, either analytically or in an iterative procedure, yields a Helmholtz-type partial differential equation for the free-surface elevation.

A simplified version of the procedure (linear equations without the Coriolis acceleration) is applied to Knight Inlet, British Columbia, a long, deep, narrow, steep-sided fjord. The extraction of tidal energy through internal mechanisms associated with the flow over the sill is represented by a body force proportional to the depth-mean velocity divided by the local time-mean depth. Computed results for the semidiurnal barotropic tidal flow agree fairly well with all available observations. An attempt to solve the same problem with a conventional time-stepping procedure demonstrates the efficiency of the harmonic approach.

When the Coriolis term is retained in the momentum equation, the *a priori* specification of a dynamically consistent surface elevation across the open boundary is difficult. Therefore, a different boundary condition (specification of flow direction along the mouth of the estuary, and of tidal height at one point thereon) is proposed and incorporated in the variational formulation of the Kelvin wave

problem. The strategy provides a means to eliminate a spurious "half-eddy" produced across the open boundary by inconsistent conditions; it also results in a cross-channel phase difference at the mouth that is consistent with other estimates and with the value measured at a nearby location. It is conjectured that Poincaré waves generated at the sill and decaying away from it might be responsible for the significant cross-channel motions observed in the vicinity of the sill.

1 INTRODUCTION

The theme of this study is the problem of calculating the motion induced by oceanic tides in semi-enclosed basins such as bays or estuaries; this is a time-dependent, boundary-value problem over a finite spatial domain. Attention will be restricted to situations where depth-averaged equations of motion can be regarded as adequate or their solution informative. The problem is then defined by the conventional set of vertically-integrated, time-dependent equations expressing conservation of horizontal momentum and mass in two dimensions. Appropriate conditions are prescribed along the shoreline boundaries and across the mouth of the estuary.

Over the past two decades, the availability of ever faster and "larger" digital computers, together with the development of novel numerical techniques, has opened many avenues of research for scientists and engineers concerned with the computation of tidal motions in coastal zones. A number of procedures has been established to solve, approximately, the classical set of shallow water wave equations for basins of realistic geometrical and topographical configurations. The most conventional approach utilizes a time-stepping procedure to handle the discretization of time in the governing equations. Spatial discretization schemes based on finite difference theory have been used by the pioneers of the field (e.g., Hansen, 1956; Brettschneider, 1967; Leendertse, 1967) and their many followers (e.g., Heaps, 1969; Ramming, 1976; Ronday, 1976; Maier-Reimer, 1977; Crean, 1978). More recently, the finite element method of spatial approximation has also been implemented in tidal flow calculations (e.g., Grotkop, 1973; Connor and Wang,

1973; Taylor and Davis, 1975; King, Norton and Iceman, 1975; Brebbia and Partridge, 1976; Gray, 1977; Walters and Cheng, 1978). In both cases, the problem is reduced to a system of first-order ordinary differential equations involving grid point or nodal values of the unknowns and their derivatives with respect to time. A considerable amount of attention has been devoted to the problem of devising time-stepping schemes that ensure the basic stability of the scheme as well as its accuracy (e.g., Ronday, 1976; Gray and Lynch, 1977). Some ingenious methods have been proposed and many applications have achieved a rather convincing degree of success. However, from a computational point of view, a common feature of the time-stepping procedures is that they are fairly expensive, even by today's standards, especially in deep bodies of water where initial transients are not rapidly damped by friction and/or radiation. An alternative approach is clearly desirable.

The time-stepping approach to the solution of time-dependent equations is appropriate when the response of the system under study is truly of a transient nature (e.g., storm surges or tsunamis). The same can be said of the method of characteristics, which is discussed, for instance, by Dronkers (1964). However, the tidal response of coastal waters was known to be predictable to a large extent due to its repetitive character long before a scientifically plausible explanation of the phenomenon was put forward. (As noted by Darwin (1898, p. 76), ancient Chinese writers considered water the blood of the Earth, and the tides the beating of its pulse.) Large-scale tidal motions are essentially "periodic" because they are due to the combined attractions of the moon and the sun on the

waters of the oceans; their coastal manifestations are also "periodic," usually with the addition of higher harmonics excited through various nonlinear mechanisms. This premise is the foundation of much theoretical (analytical) work concerning tides; it is also the basis of an approach to practical computations in which time is eliminated as an independent variable.

In the late 1860's, building upon the work of Newton, Bernoulli, and Laplace, Thomson (Lord Kelvin) proposed the theory of harmonic analysis of the tides based upon the development of a sum of periodic terms. The harmonic or Fourier method has been used ever since in the analysis of tidal data and the construction of tide tables. Also, the numerical solution of Laplace's tidal equations over large domains (i.e., the computation of oceanic wave motion directly induced by astronomical forcing) is usually carried out in terms of the major tidal constituents (see Hendershott, 1977, for a recent review): the hyperbolic tidal equations are thereby reduced to a system of elliptic equations. The implementation of the harmonic method in the calculation of tidal motions in coastal waters and rivers is discussed by Schönfeld (1951) and Dronkers (1964), the latter giving special attention to the linearization of the quadratic resistance term of the momentum equation. Until recently, however, the method of spectral decomposition seems not to have been extensively used in conjunction with numerical techniques to solve the shallow water wave problem in two horizontal dimensions, with boundary forcing. Pearson and Winter (1977) formulated an approach to tidal computations that combines the use of Fourier analysis, an iterative technique, variational calculus, and the finite element method. At the same time, Kawahara and his co-

workers (1977, 1978) applied the so-called "Periodic Galerkin Finite Element Method" to the same problem, resorting to either a perturbation or an iterative method to linearize the equations. Le Provost and Poncet (1978) started with a harmonic, rather than Fourier, decomposition of the solution, linearized the frictional term and used a finite element method to solve a variational principle equivalent to the resulting elliptic equation. Snyder *et al.* (1979) also chose the harmonic representation for their (finite difference) model and they handled the coupling of the various constituents by means of an iterative scheme. In conclusion, the elimination of the time variable by spectral decomposition of the equations of motion constitutes a sound and attractive alternative to the conventional approach.

In the next chapter, the computational procedure proposed by Pearson and Winter (1977) and the simpler linear version described by Jamart and Winter (1978) are summarized. Chapter 3 is devoted to a discussion of the application of the linear procedure to Knight Inlet, a long, deep, narrow, steep-sided fjord with relatively shallow sills located in British Columbia, Canada. Model results are compared to available field data, and an attempt to use a conventional time-stepping procedure to compute the tides in Knight Inlet is briefly described. In Chapter 4, certain problems which arise when the Coriolis term is restored in the equation describing the conservation of horizontal momentum are discussed. Finally, conclusions and suggestions for future work are set forth in Chapter 5.

2 FINITE ELEMENT SOLUTION OF THE SHALLOW WATER WAVE EQUATIONS IN FOURIER SPACE

The equations governing barotropic tidal motions in estuaries are the well-known set of vertically-integrated, time-dependent equations expressing conservation of horizontal momentum and mass in two dimensions [see, for example, Leendertse (1967)]. In its most general formulation, the momentum equation includes convective acceleration, Coriolis acceleration, and terms describing the effect of wind stress and bottom friction. The equation expressing the conservation of mass is also nonlinear. The conventional condition on Γ_1, the seaward boundary of the estuary is the specification of the free-surface elevation as a function of time and position; it is assumed in this and the next chapter that such specification is indeed possible. Along the shoreline, denoted by Γ_2, the normal velocity is prescribed (usually zero, except when river runoff is included). This chapter consists of a review of the approach pro-proposed by Pearson and Winter (1977) for the solution of these equations, and of the simpler version of that procedure subsequently developed by Jamart and Winter (1978).

The computational method described in the first of these papers is applicable to the general formulation of the problem. The simplified version of that procedure is appropriate for cases in which Coriolis and advective accelerations and wind stress can be neglected and the frictional force assumed linear. In both cases, the assumption is made at the outset that the solution is periodic in time. Therefore, the dependent variables [$\underset{\sim}{u}(x,y,t)$, the depth-averaged

velocity, and $\zeta(x,y,t)$, the free-surface elevation above mean sea level] can be Fourier decomposed. Let ω be the fundamental circular frequency of the motion and let N denote the number of modes required to describe the temporal variation of the variables. By introducing in the time-dependent equations of motion the series expansions

$$\underset{\sim}{u} = \mathrm{Re} \sum_{n=0}^{N} \underset{\sim}{U}_n(x,y)e^{-in\omega t} \tag{1}$$

$$\zeta = \mathrm{Re} \sum_{n=0}^{N} H_n(x,y)e^{-in\omega t} \quad , \tag{2}$$

the governing equations are replaced by a set of modal equations of the form

$$-in\omega \underset{\sim}{U}_n + g\underset{\sim}{\nabla} H_n = \underset{\sim}{\psi}_n^{(1)} \tag{3}$$

$$-in\omega H_n + \underset{\sim}{\nabla} \cdot (D\underset{\sim}{U}_n) = \psi_n^{(2)} \quad , \tag{4}$$

where $D(x,y)$ is the time-mean depth, g denotes the acceleration due to gravity, and $\underset{\sim}{\nabla}$ is the gradient operator. The variable $\underset{\sim}{\psi}_n^{(1)}$ is defined as the n-th complex coefficient of the Fourier series of the sum of all the terms retained in the momentum equation but two: the local acceleration and the pressure gradient term. In a similar fashion, $\psi_n^{(2)}$ represents the n-th Fourier coefficient of the non-linear term of the continuity equation. In both procedures, these variables are handled by means of an iterative scheme, i.e., they are considered known functions of position at each step of the calculations. In the method of Pearson and Winter, the distinct modal equations are coupled through the ψ_n's due to the presence of the nonlinear terms. Many authors have discussed the linearization of the term representing bottom friction in the shallow water wave equations

(e.g., Dronkers, 1964, p. 271 *et seq.*; Ippen and Harleman, 1966, p. 504). In the simplified approach of Jamart and Winter (1978), the frictional force is assumed to be proportional to the velocity divided by the local time-mean depth; with E denoting a (constant) dissipation coefficient, we have

$$\underset{\sim}{\psi}_n^{(1)} = -\frac{E}{D}\underset{\sim}{U}_n \tag{5}$$

$$\psi_n^{(2)} = 0 \quad , \tag{6}$$

so that there is no coupling between harmonics. Fourier decomposition is also performed on the boundary equations. If the shoreline boundary is impermeable everywhere, this leads to

$$H_n(x,y) \text{ given on } \Gamma_1 \tag{7}$$

$$\underset{\sim}{U}_n \cdot \underset{\sim}{n} = 0 \text{ on } \Gamma_2 \quad , \tag{8}$$

where $\underset{\sim}{n}$ is the outward-directed unit normal vector. The next step in both procedures consists of eliminating $\underset{\sim}{U}_n$ between (3) and (4) to derive a (complex) Helmholtz equation for H_n. In the linearized version, we get

$$\underset{\sim}{\nabla} \cdot (D\underset{\sim}{\nabla}H_n) + \frac{n^2\omega^2}{g} H_n = -\frac{in\omega E}{gD} H_n - \frac{E^2 + in\omega ED}{E^2 + n^2\omega^2 D^2}\underset{\sim}{\nabla}D \cdot \underset{\sim}{\nabla}H_n \quad , \tag{9}$$

and the boundary condition condition (8) becomes

$$\frac{\partial H_n}{\partial n} = 0 \text{ on } \Gamma_2 \quad . \tag{10}$$

Pearson and Winter's equation for H_n has a right-hand side that cannot be evaluated analytically and is therefore treated numerically throughout the iterative procedure. For each mode, the complex

problem is rephrased in terms of a variational principle that is then solved by means of a finite element method. The same strategy is adopted in the simplified version because the complete equation (9) appears not to be amenable to a variational formulation due to the form of its right-hand side term. Furthermore, in order to facilitate the handling of a large number of nodal points on the computer, equation (9) is separated into its real and imaginary parts, setting

$$H_n = h_n + is_n \quad . \tag{11}$$

This leads to a pair of non-homogeneous (real) Helmholtz equations. Each problem is then recast in terms of the well-known corresponding variational principle: for instance, if F_n denotes the real part of the right-hand side of (9) and A the area enclosed by Γ_1 and Γ_2, h_n is given by

$$\delta \int_A \left(\frac{D}{2} |\nabla h_n|^2 - \frac{n^2 \omega^2}{2g} h_n^2 + F_n h_n \right) dA = 0 \quad , \tag{12}$$

for all δh_n vanishing on Γ_1. The forcing term F_n is a functional of D, h_n, $\frac{\partial s_n}{\partial x}$, and $\frac{\partial s_n}{\partial y}$; it is known in the sense that its value is estimated from the results of the previous iteration. A standard finite element method is used to obtain the approximate solution of each variational problem. After convergence of the iterative process has been achieved, the Fourier coefficients of the velocity, $\underset{\sim}{U}_n$, are computed from equation (3).

The linearized version of the approach just described is somewhat easier to implement on a computer than the more general version for several reasons. First, it does not involve coupling between the different modes of the solution, thereby alleviating storage require-

ments. Second, the calculation of the velocities (i.e., essentially the derivatives of the free-surface elevation) is not needed during the iterative process but only after convergence is achieved; this is an advantage as long as linear basis functions are used to describe the elevation. Moreover, the same coefficient matrix is used for the determination of h_n and s_n, and the matrix decomposition need be done only once because only the right-hand sides are updated iteratively.

In the next chapter, the utility of the simplified procedure in specific situations is evaluated by means of an application to a deep fjord. Because only one Fourier mode of the total response will be considered, the subscript n will be omitted hereafter.

3 APPLICATION TO KNIGHT INLET

INTRODUCTION

Knight Inlet (Figure 1) is a long, deep, narrow fjord with steep sides and relatively shallow sills. It is located on the southern mainland coast of British Columbia, Canada, its mouth facing the northern part of Vancouver Island. The general characteristics of Knight Inlet have been described in detail by Pickard (1956, 1961) and Pickard and Rodgers (1959); these authors consider Knight Inlet typical of fjords along the British Columbia Coast. Knight Inlet is more than 100 km long, and it has an average width of about 3 km. It has two sills: an outer threshhold located 10 km west of Montagu Point, and an inner one lying between Hoeya Head and Prominent Point. The latter sill has a maximum depth of about 63 m and separates a very deep inner basin (maximum depth of 550 m) from a somewhat shallower ($\simeq$ 200 m) outer basin. The inner sill is located near the middle of a fairly long straight section of the fjord. Because its topography is relatively simple, this segment of Knight Inlet was chosen as the site for extensive field programs (Smith and Farmer, 1977; Farmer and Smith, 1978; Freeland and Farmer, 1980). The main reason and incentive for the initiation of tidal modeling in this particular inlet was the prospect of comparing model calculations with reliable field data. It also seemed desirable to determine the usefulness of the linearized model in a deep fjord with a rather shallow sill.

At times of high freshwater runoff, Knight Inlet becomes strongly stratified, and the phenomena associated with the density structure have been the focus of the investigations just mentioned. Of particular relevance to the present attempt to compute the barotropic

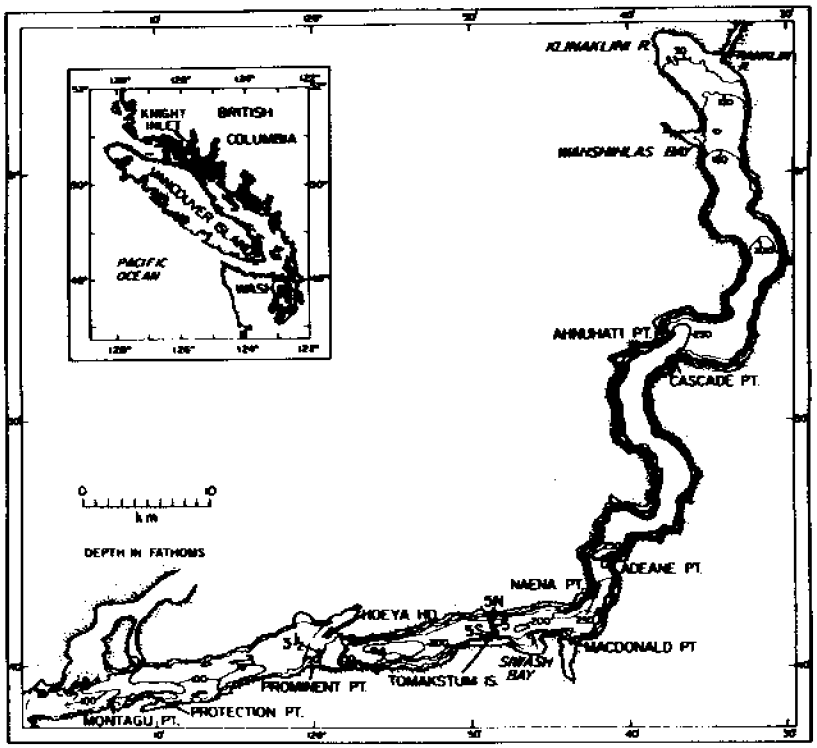

Figure 1. Map of Knight Inlet, British Columbia. The inset shows the fjord's location on the British Columbia coastline. The dots in the straight reach indicate locations where tidal currents have been measured; the numbering of the stations is consistent with traditional notations employed in Knight Inlet.

tidal motion is a point made by Freeland and Farmer (1980): namely, that a significant portion of the tidal energy appears to be extracted in the sill region through certain internal mechanisms which result in the formation of internal solitary waves (Smith and Farmer, 1977; Farmer and Smith, 1978; Maxworthy, 1979). An accurate parameterization of those complex internal phenomena, for use in vertically-integrated equations of tidal motion, is probably not yet possible and certainly beyond the scope of this study. (A quantitative description of such "dissipation" as a function of time would require careful consideration of, at least, velocities and hence amplitude of the tide, vertical shear, and nature and strength of

stratification; also it would probably involve "switches" to allow for episodic occurrences of instabilities and sudden changes in the flow regime). However, there appears to be no compelling reason why this type of dissipation should be modeled by the classical quadratic friction law.

As a first approximation, the working assumption is made that, in tidal computations, the internal energy dissipitation could be modeled by the "frictional" term of equation (5). This term acts as a body force and it has the property that the "momentum sink" is maximum over the sill where the mid-channel depths are shallowest and where, from mass continuity alone, one expects the velocities to be largest. The dissipation coefficient, E, is adjusted so as to best approximate what is known about the change of phase of the tidal elevation along the inlet.

In the sections which follow, the finite element discretization of Knight Inlet is described first. Next, the adjustment of E is discussed, and the computed results are presented. Then, the model results are compared with available field data. The next section is devoted to some numerical considerations. Finally, an attempt to use a time-stepping procedure to solve the same problem is reported.

SPATIAL DISCRETIZATION

The finite element grid which was first used for Knight Inlet (Figure 2) extends from Protection Point to the head of the inlet. The grid is composed of 1584 triangular elements (997 vertices or nodal points), and the variables (h and s) as well as the depth are assumed to vary linearly over each triangle. The shoreline boundary follows the 5 fathoms (≈ 10 m) contour. Figure 3 shows the topography of Knight Inlet after digitization (the contouring program

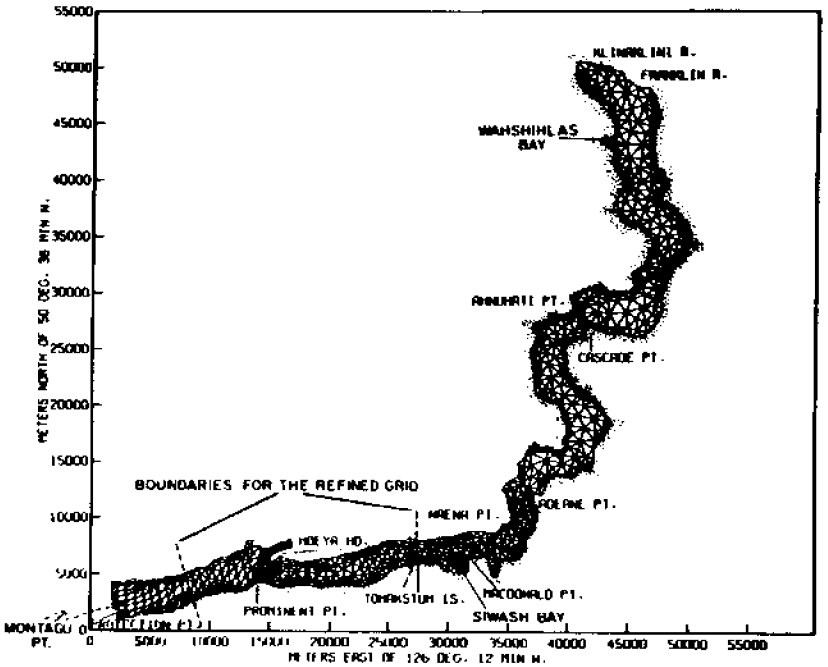

Figure 2. Finite element grid used in first phase of calculation of barotropic tidal flow in Knight Inlet (after Jamart and Winter, 1980).

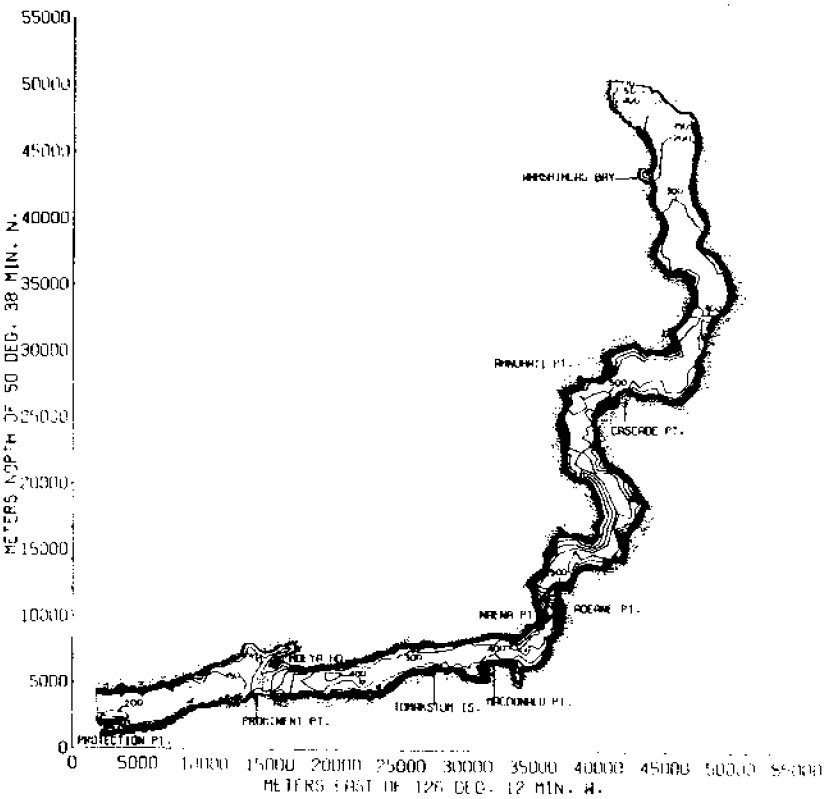

Figure 3. Approximation to the bathymetry of Knight Inlet, as used in the calculations.

that generated this plot uses linear interpolation between depth data at the nodal points).

A second grid was constructed because the velocity field obtained with the first grid lacked smoothness in the sill region, especially at times close to the ebb-flood transition, thereby indicating the need for better spatial resolution in that area of rapid variations. The refined grid (Figure 4) covers a portion of the straight reach that includes the sill, and it was generated by joining the mid-side points of the original triangles; the element density is thereby quadrupled. An algorithm designed to minimize the bandwidth of the algebraic problem was used to number the nodes of the refined grid. An alternative mesh refinement scheme (joining the vertices of each triangle to the centroid) was judged unsatisfactory because it led to rather small angles. The new grid has two open boundaries (see Figure 2) and the motion in the interior of the domain is driven by specifying on those boundaries the elevations computed with the coarser grid. The depth values at the additional nodal points are linearly interpolated from the first grid's data so that the actual mean volume of the section remains unchanged.

ADJUSTMENT OF THE DISSIPATION COEFFICIENT

In order to study the effect on the solution of varying the dissipation coefficient, E, a number of runs was made for a wave of amplitude $(h^2 + s^2)^{\frac{1}{2}} = 2$ m on Γ_1 and of period $T_p = 12.5$ h. Those experiments showed that the calculated phase difference in elevation, $\Delta\Phi$, between the head of the inlet and the open boundary of the model, Γ_1, is almost linearly proportional to E, at least up to a value of $E = 5 \times 10^{-2}$ m sec^{-1} (see Table 1, col. 2). Moreover, the longitu-

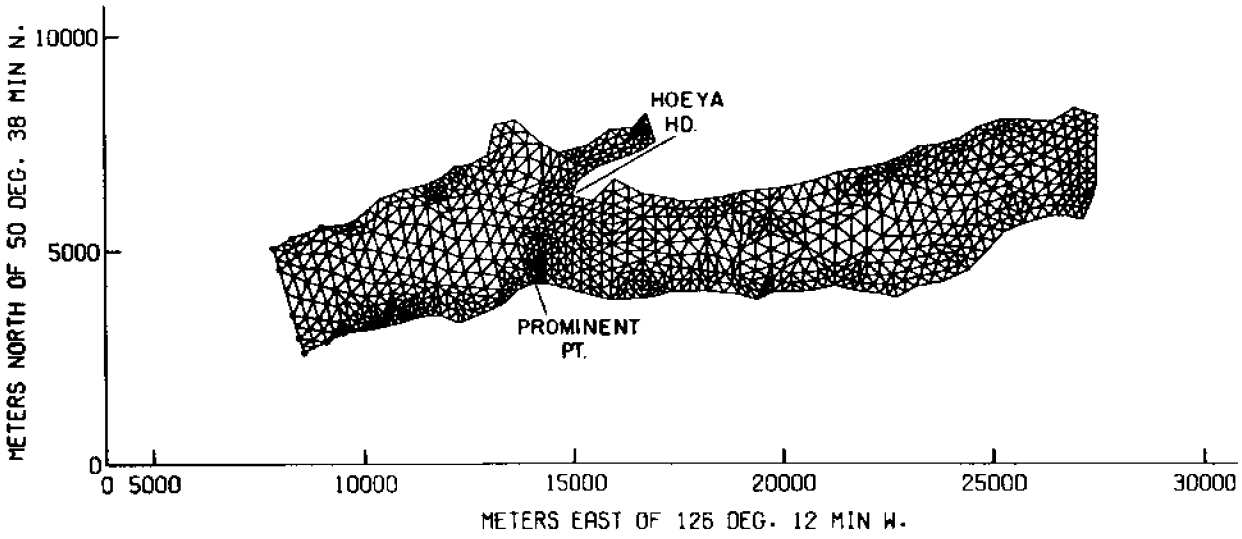

Figure 4. Fine resolution finite element grid for computations in the vicinity of the sill (after Jamart and Winter, 1980).

dinal distribution of Φ relative to Γ_1 shows a very abrupt change of slope in the sill region (see Figure 7b for a typical profile of Φ). Consequently, the delay observed at the head of the fjord (relative to Γ_1) is caused mainly by the dissipation occurring over the sill (i.e., the linearized model formulation does provide the intended parameterization of the physics).

This last result is consistent with the tide gauge data described by Freeland and Farmer (1980), who analyzed long-term records obtained at three locations: Montagu Point (a few km west of Γ_1), Siwash Bay, and Wahshihlas Bay (see Figure 1), hereafter referred to as M, S, and W. At tidal frequency M_2, the observed phase difference between Siwash Bay and Montagu Point, $\Phi_S - \Phi_M$, fluctuates between values of 0.75^o (January) and 1.7^o (June) whereas the difference between Wahshihlas Bay and Siwash Bay, $\Phi_W - \Phi_S$, remains smaller than 0.25^o. The statistical significance of such estimates is discussed by Freeland and Farmer (1980). The large discrepancy between these phase differences will be reflected in estimates of energy dissipa-

tion rate over the straight section and the sinuous reach and this, indeed, is one of the main arguments that led Freeland and Farmer to the assertion quoted in the introduction to this chapter. The phase observations can be well simulated in the computations by selecting an adequate value of E, as shown by columns 3 ($\phi_S - \phi_{\Gamma_1} = \phi_S - \phi_M$) and 4 of Table 1. These phase differences are computed for an M_2 wave whose amplitude on Γ_1 is different from the observed one but they are independent of that amplitude. Therefore, the choice $E = 1 \times 10^{-2}$ m sec^{-1} yields a good approximation of the average phase observation.

Table 1: Calculated phase differences and number of iterations for various values of the dissipation coefficient.

E (m sec^{-1})	$\Delta\phi$ (degree)	$\phi_S - \phi_{\Gamma_1}$ (degree)	$\phi_W - \phi_S$ (degree)	Number of Iterations
0	0	0	0	2
3×10^{-3}	0.480	0.411	0.065	3
6×10^{-3}	0.877	0.749	0.119	6
1×10^{-2}	1.37	1.17	0.19	10
1.5×10^{-2}	1.97	1.69	0.26	16
3×10^{-2}	3.74	3.24	0.46	26
5×10^{-2}	6.07	5.29	0.72	28

RESULTS

The most striking features of the results occur, as expected, in the neighborhood of the sill. However, unlike the longitudinal distribution of the phase described above, the other two main features of the solution are present for all values of E, including E = 0. The first characteristic is a rather large increase in the magnitude of the current speed and is shown, for example, in Figures 5 and 6, where the velocity vectors in the sill region are plotted on a scale differ-

ent from that used for the other parts of the inlet. (Note that the scales also differ from figure to figure.) In those figures, as well as in subsequent displays of the velocity field, the parameter α denotes the non-dimensional time, $\alpha = t/T_p$; the time origin was chosen such that ζ is maximum on Γ_1 at $\alpha = 0.125$ for computational reasons discussed in "Numerical Considerations." The variation of mean current speed with depth is merely a consequence of the continuity equation: neglecting spatial variations in H, the one-dimensional

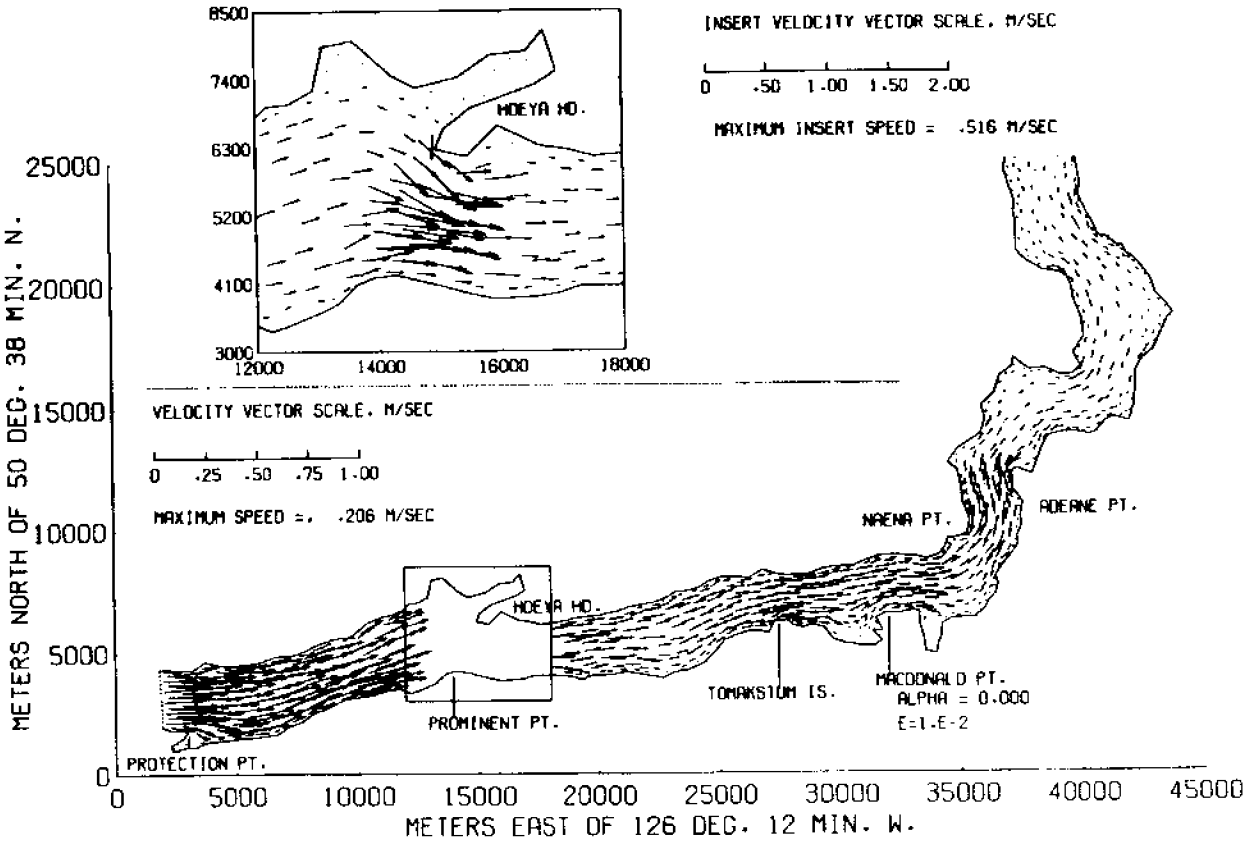

Figure 5. Velocity vector field calculated on the global grid at $\alpha = 0$, i.e., one-eighth of a period before maximum tidal height at the entrance.

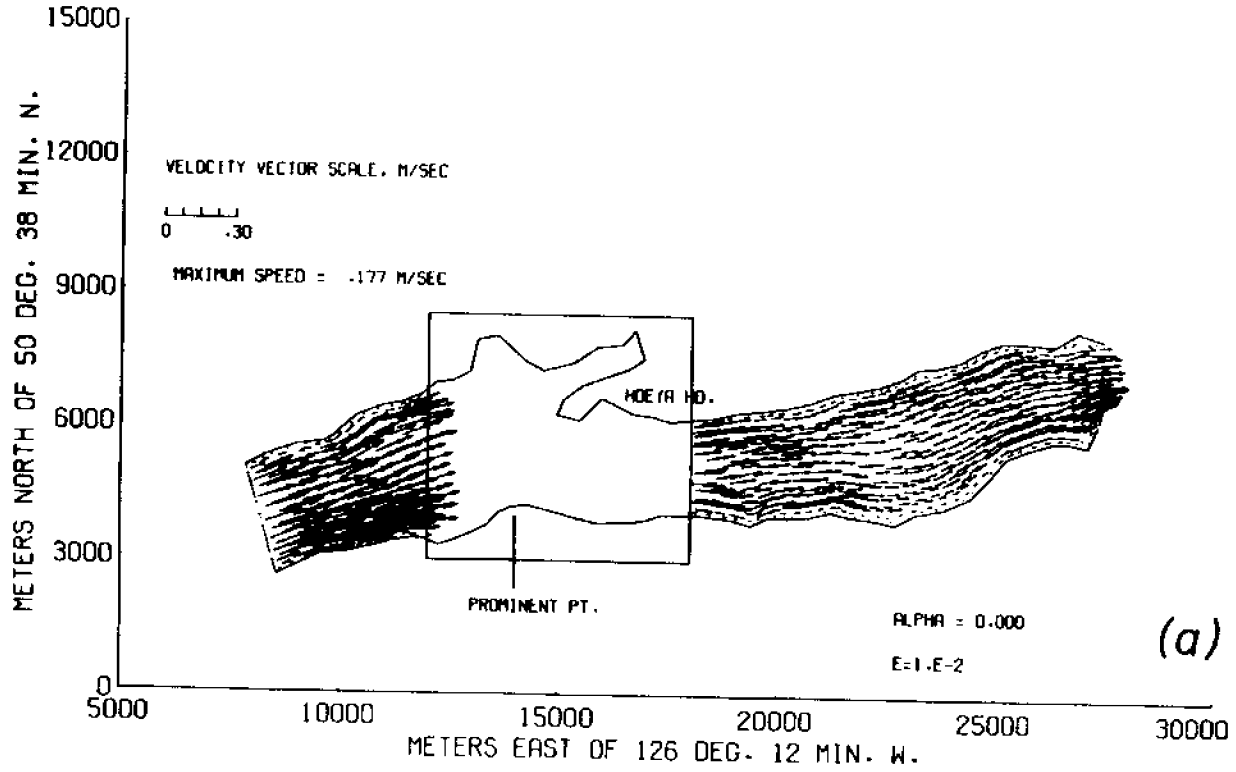

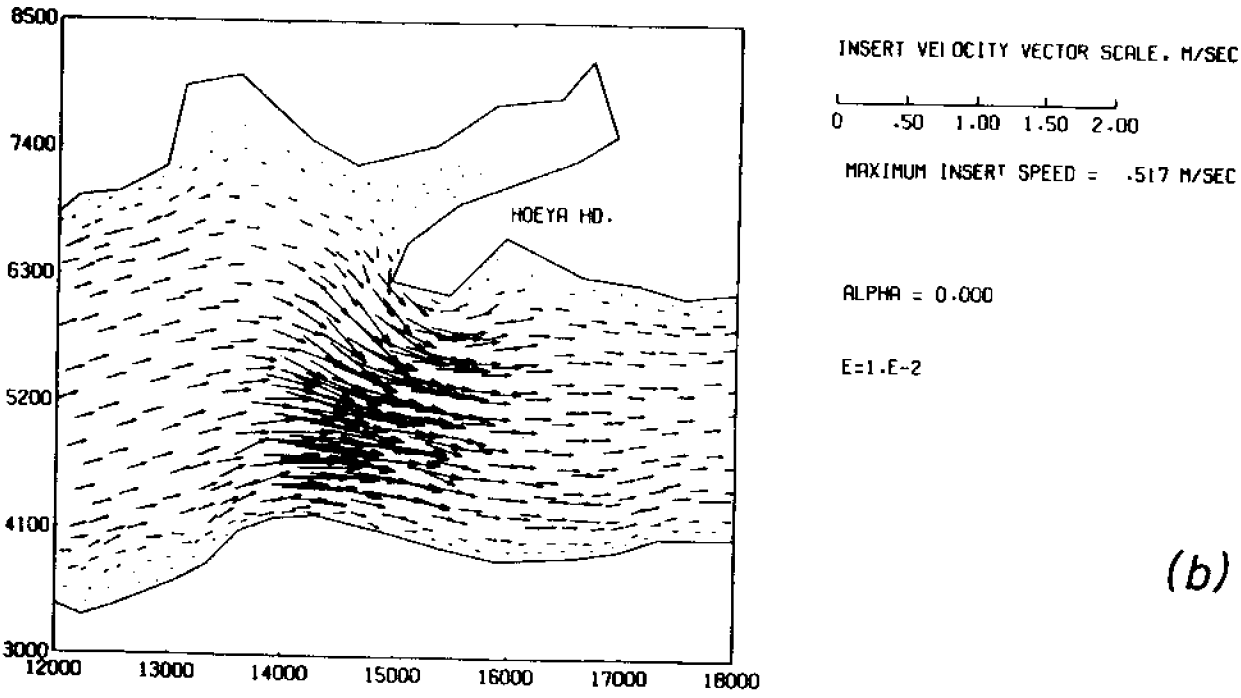

Figure 6. Velocity vector field calculated on the refined grid at $\alpha = 0$. a) straight reach b) mill area

equivalent of equation (4) that shows that $|\underline{U}|$ is inversely proportional to the depth D.

The second feature of the solution over the sill is the surface manifestation of the velocity increase, namely, the presence in that region of a relatively large longitudinal gradient in the magnitude of the elevation. This feature spans only a few elements of the global grid, but the same "bump" is present when the calculations are performed on the refined grid; therefore it is unlikely to be a numerical artifact. Figure 7a shows the profile of $(h^2 + s^2)^{\frac{1}{2}}$ for a wave of amplitude 1.5274 m on Γ_1 and of period 12.5 h, computed with $E = 1 \times 10^{-2}$ m sec^{-1} but indistinguishable, on this scale, from the solution for $E = 0$. The shape of the solution can also be explained in terms of a partial wave reflection due to the sill (M. Rattray, Jr., personal communication). Figure 7b shows the corresponding distribution of phase relative to Γ_1, a profile discussed in the previous section; obviously, there is no phase change in the elevation for the case $E = 0$. The depth profile along the same mid-channel axis is included in Figure 7c for reference. Over most of the tidal cycle, the free-surface profile defined by Figures 7a and 7b is characterized by an inflection point near the sill. However, at certain times (about one-eighth of a period after the time of maximum currents) there appears a local maximum or minimum in elevation centered at the sill; as an example, Figure 7d shows the shape of the free surface at $\alpha = 0$, i.e., one-eighth of a period before high tide on Γ_1.

As a consequence of the inclusion of a depth-related dissipation term in equation (3), side effects are, *de facto*, modeled due to the extreme steepness of the fjord's banks. During periods of

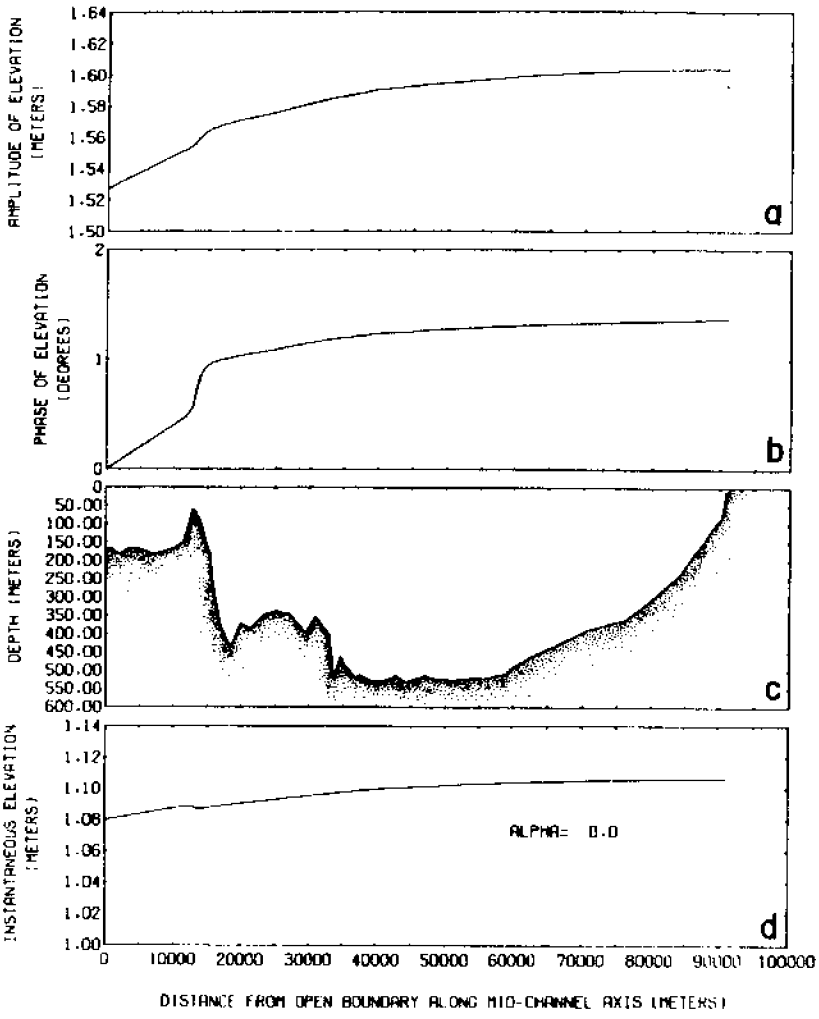

Figure 7. Longitudinal profiles of surface elevation and depth along the mid-channel axis.

a) calculated amplitude of the free-surface elevation
b) calculated phase of the free-surface elevation
c) bathymetry used in the calculations
d) free-surface elevation one-eighth of a period before maximum tidal height at the entrance

unidirectional flow, the relative shallowness of the boundary elements is responsible for a marked shear on both sides of cross-sectional velocity profiles. The progressive decrease in the magnitude of the velocity near the solid boundary can be observed in both Figure 6 (velocity vector field at $\alpha = 0$) and Figure 8 (axes of the tidal ellipses). The magnitude of that shear increases,

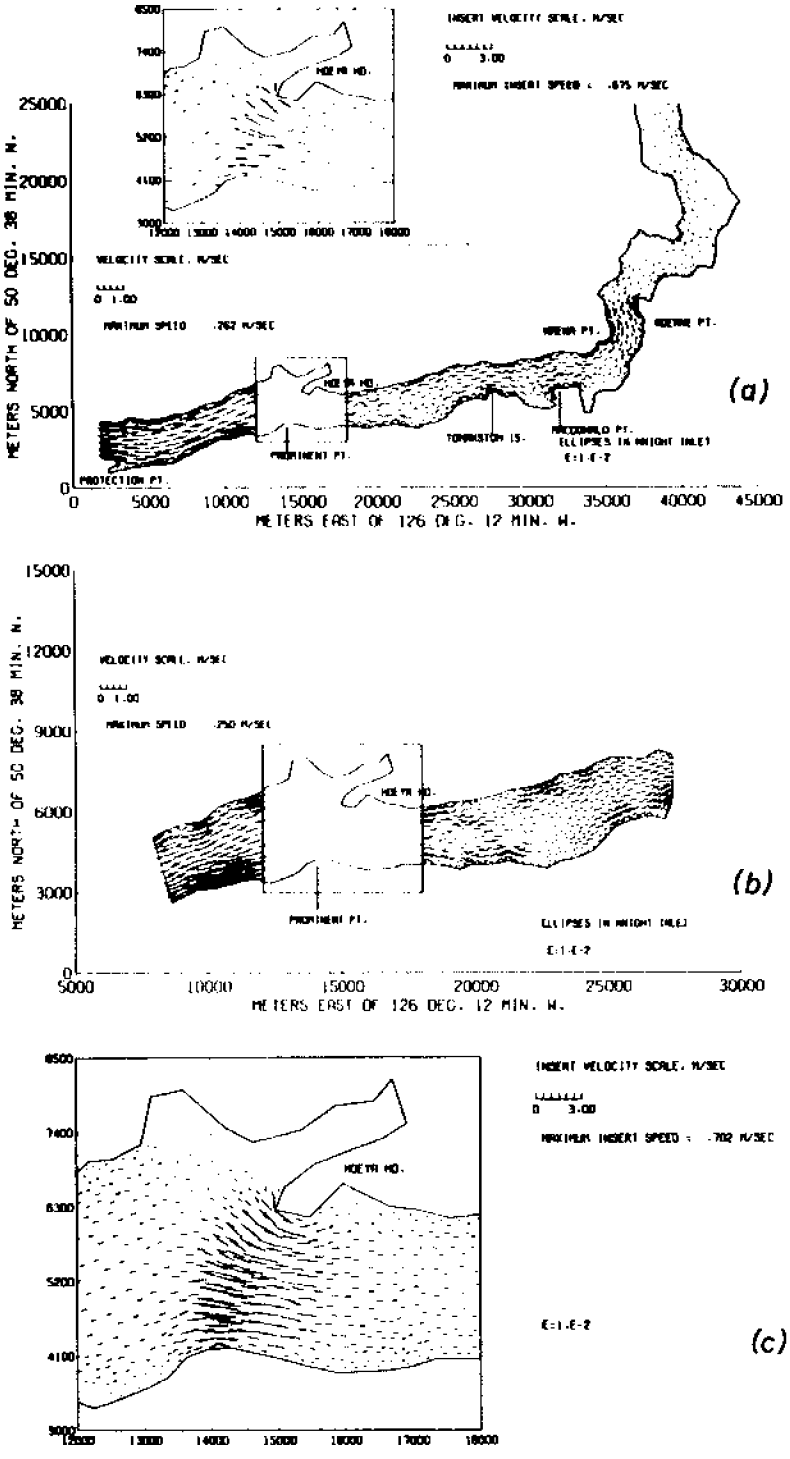

Figure 8. Axes of the M_2 tidal ellipses in Knight Inlet, calculated with a dissipation coefficient E = 1 x 10^{-2} m sec^{-1}.

a) coarse grid
b) refined grid, straight reach
c) refined grid, sill area

of course, with increasing E. Also, the larger resistance associated with the boundary elements produces cross-channel variations in phase (the tide "turns" first along the edges) that result in the formation of eddies during the ebb-flood transitions. This is illustrated in Figures 9 and 10 which show the tidal current patterns shortly after high tide.

COMPARISON WITH AVAILABLE DATA

Most of the results from field measurements referred to in this section have not, as of this writing, been published; they were kindly communicated by Drs. G.A. Cannon and H.J. Freeland who not only collected and analyzed the data but also contributed much to their interpretation.

Three basic limitations hinder somewhat the so-called model validation process. The first stems from the decision to test the usefulness of a purely linear model. In particular, the character of the solution in the area of the sill suggests that the convective acceleration term may not be negligible in that region; however, this drawback is intrinsic to the nature of the exercise. The second limitation is related to the objectives of the field programs recently conducted in Knight Inlet, *viz.*, the study of the internal phenomena associated with the flow of a stratified fluid over rugged bottom topography: part of the resulting data set does not possess a sufficient temporal and spatial coverage to allow the accurate calculation of the depth-averaged tidal velocities. The third difficulty is one of data interpretation; namely, the problem of extracting from the total (measured) motion that component which is the object of the modeling attempt. In spite of these limita-

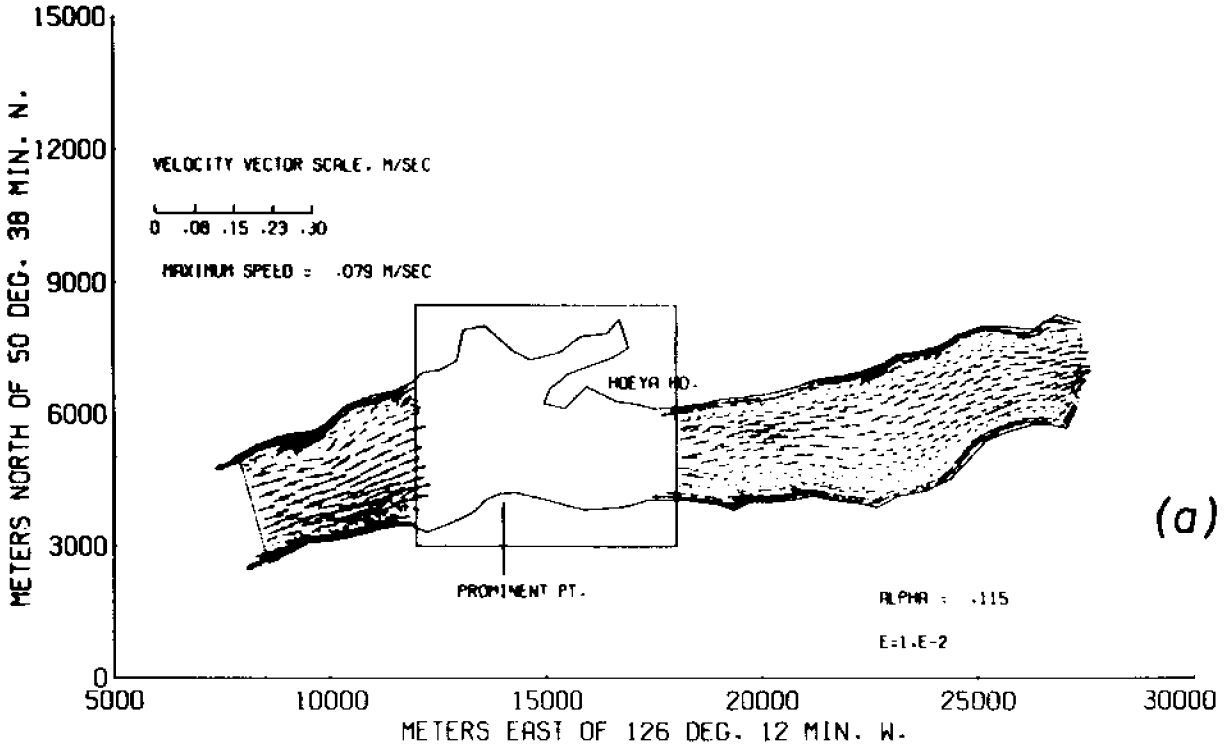

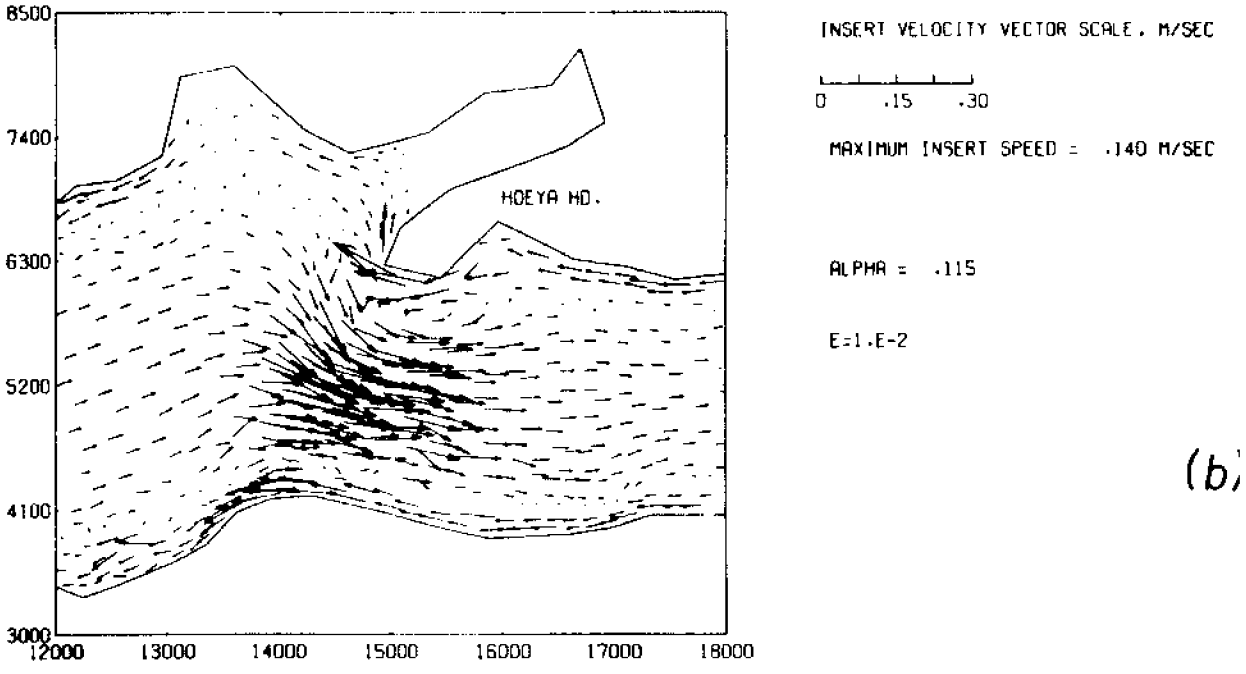

Figure 9. Velocity vector field calculated on the refined grid at $\alpha = 0.115$, i.e., one-hundredth of a period before maximum tidal height at the entrance.

a) straight reach
b) sill area

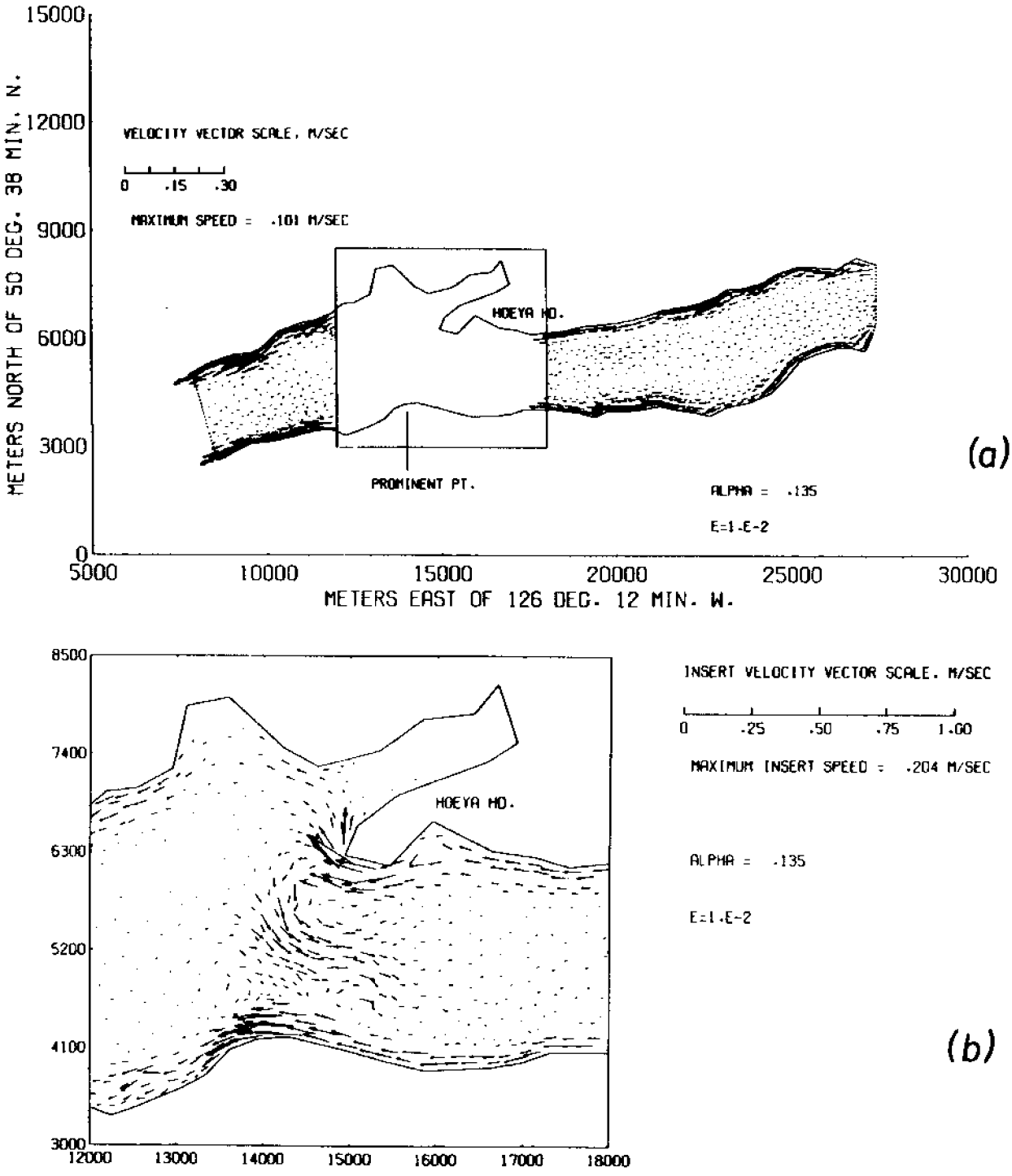

Figure 10. Velocity vector field calculated on the refined grid at α = 0.135, i.e., one-hundredth of a period after maximum tidal height on Γ_1 (after Jamart and Winter, 1980).

a) straight reach
b) sill area

tions, enough information is available to assess the general validity of the model.

In this section, attention is restricted to the tidal constituent which is dominant in Knight Inlet, i.e., the principal lunar semidiurnal (M_2) tide. Comparisons similar to those reported here between observations and model results at the diurnal frequency show the same degree of general agreement. The following comparisons are also restricted to the up- and down-inlet component of the velocity; the transverse component of current will be discussed in Chapter 4. Lastly, it should be pointed out that all the figures displaying the velocity field correspond to results obtained for a wave of amplitude equal to 2 m at the open boundary, whereas the measured elevation at the M_2 frequency is 1.5274 m (Freeland, personal communication; this value was obtained from the harmonic analysis of a one year-long time series at Montagu Point); the "calculated speeds" quoted in this section correspond to the measured forcing.

Free-Surface Elevation

As described in "Adjustment of the Dissipation Coefficient," tidal elevations have been recorded at three locations for more than a year. In the same section the adjustment of the model was discussed; i.e., choosing E so as to simulate the "average" phase information for the M_2 tide deduced from the measurements. The M_2 amplitudes computed by Fast Fourier Transform of eight 29-day time series are in the following ratios (M designates Montagu Point, S Siwash Bay, and W Wahshihlas Bay):

	W/S	S/M
mean	1.0138	1.0276
minimum	1.0127	1.0263
maximum	1.0153	1.0284

With $E = 1 \times 10^{-2}$ m sec^{-1}, the computed value of W/S is 1.0139 and agrees very well with the observed mean value; however, the calculated ratio S/M has a value of 1.0351, somewhat larger than the observed ones. Hence, it cannot be said that the "bump" associated with the sill in the profile of the computed free-surface amplitude (Figure 7a) is confirmed by the observations. Tide-gauge measurements at sites much closer to the sill would be needed to answer that question. Such data would also be useful in judging whether or not the phase difference observed between the two extremities of the straight reach is concentrated over the sill as shown in the calculated profile of Figure 7b.

Depth-Averaged Longitudinal Velocity

Figure 1 shows the locations for which some information on barotropic tidal transport is presently available. (The numbering of the stations is consistent with the traditional notations employed in Knight Inlet.)

At the westernmost station, number 3, Freeland (personal communication) estimates that the barotropic depth-mean velocity at the M_2 frequency is approximately 14 cm sec^{-1} and precedes the elevation by about 87°; the computed magnitude and phase, with $E = 1 \times 10^{-2}$ m sec^{-1}, are about 15.5 cm sec^{-1} and about 85° for a wave of amplitude 1.5274 m on Γ_1. Freeland's estimate is based on the amplitude and phase of the M_2 velocity observed at only two depths (15 m: 12.68 cm sec^{-1}, -111.05°; 100 m: 14.36 cm sec^{-1}, -92.01°); he uses the Msf data at three depths to calibrate the shape of the first baroclinic mode and subtracts the internal mode from the observations. The accuracy of such "measurement" is difficult to assess, but the agreement with the model results is satisfactory.

The amplitude of the barotropic M_2 velocity at station 5 can be deduced vectorially from the two pairs of current observations made by Cannon at stations 5_N and 5_S. The resulting value of 9.2 cm sec^{-1} is exactly the same as the calculated velocity at mid-channel; no phase measurement with respect to elevation is available. The baroclinic (residual) components of the fluctuations recorded by those four current meters suggest the presence of a standing internal Kelvin wave (Freeland, personal communication).

Attempts to estimate the depth-averaged velocity from the four instruments moored at station 4 have not been successful. However, the model result, approximately 7.5 cm sec^{-1}, is comparable to the observed longitudinal speeds (8.32, 7.90, 5.49, 7.50 cm sec^{-1} at 65, 125, 300, 363 m respectively).

The only information presently available on the magnitude of the tidal currents over the sill (station 3½) comes from the measurements reported by Pickard and Rodgers (1959). As these authors emphasize, the accuracy of their observations is greatly affected by many uncertainties due, among other things, to the natural variability and complexity of the flow and to ship motion. Moreover, no time series analysis of the data is possible because of their limited duration. However, the usefulness of Pickard and Rodgers' measurements can be tested by comparing their results for station 5 to the more recent data for the same location. With a tidal range of about 4 m, they report a mean range of longitudinal currents of about 30 cm sec^{-1} at 200 and 300 m and about 24 cm sec^{-1} at 100 and 50 m. These can be roughly converted to mean velocities of 11.4 and 9.2 cm sec^{-1}, respectively, for a wave of amplitude 1.53 m, which are very close to the value of 9.2 cm sec^{-1} mentioned earlier. Appli-

cation of a similar conversion at station 3½, where a range of speeds of 150 cm sec^{-1} was observed at a time when the tidal range was about 5 m, yields an estimate of 45.9 cm sec^{-1} for the M_2 velocity at that location; the closeness of the calculated value (46.7 cm sec^{-1}) is, of course, fortuitous, but it confirms the overall pattern of fair agreement between observations and model results.

Lastly, no current measurements were made close enough to the lateral boundaries of Knight Inlet to provide evidence for the side effects discussed at the end of the previous section, but the occurrence of such effects has been reported for other steep-sided channels. Thomson (1976, 1977) concludes from his study of currents in nearby Johnstone Strait, a fjord-like narrow tidal channel along the northeastern side of Vancouver Island, that "the M_2 constituent (exhibits) cross-channel symmetry with respect to phase in which the currents in the central part of the strait (lag) those at either shore by approximately 30° (≈1 hour)." The phase gradient is steepest in fairly narrow zones (a few hundred meters) on both sides of the channel. The transverse phase gradients that were calculated in the case of Knight Inlet are comparable to those observed in Johnstone Strait (for instance, in the vicinity of station 3, the calculated velocity along both shores leads that in the central part of the inlet by about 40°); those phase gradients and the related shear in the magnitude of the tidal velocity are concentrated along the boundary. A similar phase lead along a lateral boundary has also been observed in Hood Canal, Washington, by Shi (1978) who remarks that "it is similar in mechanism to the Stokes oscillating boundary layer in a (viscous) flow." In the case of Hood Canal, the

magnitude of the tidal velocity decreases markedly near the shore.

The conclusion drawn from such admittedly limited comparisons with field data is that the simple linearized model appears to be capable of reproducing the main features of a given tidal constituent in a deep estuary such as Knight Inlet, regardless of the exact nature of the internal dissipation processes.

NUMERICAL CONSIDERATIONS

As mentioned in Chapter 2, the numerical procedure adopted to solve, with an iterative scheme, the equations corresponding to the real and imaginary parts of equations (9) and (10), is basically the same as that reported in Jamart and Winter (1978). As a practical definition of convergence, it was decided to terminate the iteration loop when the relative change between successive estimates of both variables is smaller than a given tolerance, ε, at all nodal points. An important modification of the procedure concerns the boundary condition at the mouth, and, specifically, the partitioning of the amplitude of H, $|H| = (h^2 + s^2)^{\frac{1}{2}}$, (recall that $H = h + is$ or $\zeta = h \cos \omega t + s \sin \omega t$) between h and s. The computational scheme is faster when $|H|$ is equally distributed between h and s than when only one variable is "excited" on Γ_1. For instance, with $\varepsilon = 10^{-4}$ (and $E = 3 \times 10^{-3}$ m sec^{-1}), convergence is achieved after five iterations if $h = s = \sqrt{2}$ m at the open boundary, while it takes fourteen iterations for a similar run with $h = 2$ m, $s = 0$ on Γ_1 to converge. On a Cray-1 computer, the latter run requires 5.25 CP seconds and the former 2.60 CP seconds. [These numbers, incidentally, give some indication of the speed of the Cray-1 computer: the construction of the basic matrix of the algebraic system expressing the discrete approximation to the variational

problem (a rectangular 997 x 35 matrix) and its LU decomposition for Gaussian elimination take little more than one second of CP time.] The outcome of this comparison might be different if the convergence criterion dealt with the absolute rather than the relative change between successive iterations.

Two other factors influence the number of iterations needed to satisfy a given convergence criterion: they are the value of the dissipation coefficient, E, and (to a lesser extent) the number of Gaussian points used in the numerical integration of the (nonlinear) "forcing terms" on the right-hand side of equation (9). Column 5 of Table 1 shows how the number of iterations (with $\varepsilon = 10^{-4}$) varies with E. The last two numbers in Table 1, corresponding to $E = 3 \times 10^{-2}$ and 5×10^{-2} m sec^{-1}, should be qualified by a question mark: they indicate the number of iterations after which successive estimates of h and s vary between two "constant" values (six significant digits), apparently without further convergence until the 40th iteration, when the computation is terminated. The relative change between two successive iterations is everywhere smaller than 3×10^{-4} so that this puzzling behavior does not seriously affect the accuracy of the results.

For the problem defined by equations (9) and (10), the convergence of both variables towards their "stable" value is oscillatory with a period of two iterations and the upper and lower envelopes are monotonic after the first few iterations. Hence, the convergence of the iterative process can be accelerated in this case by using as the current value of the unknowns the mean of the last two estimates. However, the character of the convergence is different when other terms of the governing equations are considered. For

instance, the convergence is asymptotic rather than oscillatory for the "Kelvin wave equations" discussed in Chapter 4. Therefore, it appears that extrapolation schemes to accelerate convergence should be designed on an *ad hoc* basis.

Six different formulae for performing the numerical integration of the forcing terms have been compared. The programming and the numerical values of the various coefficients and weights were checked by running the computer program for a flat bottom case; the forcing terms are then linear functions of position so that the integration should be "exact," except for round-off errors. The numerical experiments show that four formulae yield essentially the same results at the same cost, and, for a tolerance $\varepsilon = 10^{-4}$, the iterative scheme converges in 3 iterations. They are given by Strang and Fix (1973, Table 4.1) and denoted (a) 13-point formula, degree of precision 7; (b) 7-point formula, degree of precision 5; (c) 6-point formula, degree of precision 3; and (d) 3-point formula, degree of precision 2, all three points being inside the triangle. [Note that there is a misprint in the first weight of (b) and in the last area coordinate value of (a).] The 3-point formula that involves the mid-side points requires five iterations and is rather inaccurate (e.g., it gives a phase difference over the total length of the inlet, $\Delta\Phi$, equal to 0.601° for $E = 3 \times 10^{-3}$ m sec^{-1} and $\varepsilon = 10^{-4}$, whereas the 13-point formula yields $\Delta\Phi = 0.480^{\circ}$). If the integration scheme uses the nodal values of the forcing function, the iterative procedure diverges in the case of Knight Inlet. With the exception of the experiments concerning the partitioning of $|H|$ between h and s, all results reported in this chapter were obtained with the 13-point formula.

The experiments just described were performed with the coarse

grid shown in Figure 2. The solution on the refined grid of Figure 4, which has two open boundaries along which the elevation is specified, requires at most three iterations. Also the discrepancies between the results obtained with the 3-point integration formula (mid-side points) and those calculated with the 13-point formula are much smaller on the fine grid than on the coarse one.

COMMENTS ON THE APPLICABILITY OF A TIME-STEPPING PROCEDURE

The efficiency of the modal decomposition approach as compared to a time-stepping procedure is illustrated in this section. To this end, the numerical model developed by Connor and Wang (and described in their joint publications of 1973, 1974, 1975) was applied to Knight Inlet. The model used is designated as CAFE-1 [Circulation Analysis (using) Finite Elements, one-layer model], and the computer code was made available through the services of the Massachusetts Institute of Technology Sea Grant Program (see reference MIT/Marine Industry Collegium). The CAFE-1 model is designed to solve a set of equations that differs from the usual shallow water wave equations by the inclusion of horizontal internal stress terms, modeled by means of "eddy" viscosity coefficients. The equations are transformed to their so-called weak form (a process akin to a formulation based on the method of weighted residuals) on which the finite element method is applied (linear triangular elements). Wang and Connor (1975) have considered several different schemes for the time integration of the resulting system of ordinary differential equations and they selected a "time-split" procedure (in which the variables, i.e., discharges and total depths, are calculated at alternating time steps) for use in CAFE-1.

Several applications of the model for the calculation of tidal and wind-driven circulations in real systems exemplify its usefulness. Wang and Connor (1975) describe three case studies, of which the most detailed one is the application to Massachusetts Bay. [Incidentally, it appears from their discussion that the real purpose of the inclusion of the lateral viscous terms is to ensure numerical stability or, in some instances, to smooth out short-wavelength noise.] Other illustrations include the application of CAFE-1 to the Great Bay estuarine system (Celikkol and Reichard, 1976) and to part of Biscayne Bay (Swakon and Wang, 1977).

As might be expected in a pioneering enterprise of such complexity, the procedure developed by Connor and Wang is not flawless. Several pertinent remarks can be found, for instance, in Lynch's (1978) critical review of the recent literature on this topic. In the present study, various computations with CAFE-1 of linear, frictionless long waves in rectangular basins of constant depth have led to the conclusion that the numerical solutions obtained with this program are rather inaccurate. The main problem, however, is the necessity of using a fairly small time-step in order that the scheme be stable. This was recognized by Wang and Connor (1975, p. 127) who could not explain why the split-time procedure, found analytically to be "linearly unconditionally stable as an initial value problem," is actually unstable in practice when the effective time-step exceeds the Courant-Friedrichs-Lewy constraint by about 50%. According to Lynch (1978), the appropriate stability constraint for this scheme is the same as for the leapfrog method; the criterion is nearly identical to that "experimentally" derived by Wang and Connor. Thus, for practical purposes, the time-step used in CAFE-1

is approximately constrained by the condition

$$2\Delta t \leq \Delta t_{cr} = \frac{\Delta s}{\sqrt{2gD}} \quad ,$$

where Δs is the grid size and D the depth of the water. In the case of Knight Inlet the combination of high resolution (i.e., small Δs) and large depth leads to the requirement of an exceedingly small time-step. Starting from rest and using the "coarse" grid of Figure 2, with $\Delta t = 10$ seconds, the procedure is unstable after about 400 seconds; with $\Delta t = 5$ seconds, no instability occurs during the first 800 seconds of the integration. If one assumes that the latter time-step is small enough to carry out the calculations in Knight Inlet, approximately one hour of CP time on the Cray-1 computer would be needed to cover a single M_2 period! This figure does not compare favorably with the CP times required by the procedure described in this study (less than 10 seconds, see "Numerical Considerations"). Hence, the application of CAFE-1 to Knight Inlet was aborted.

4 REMARKS ON THE EFFECT OF THE EARTH'S ROTATION

STATEMENT OF THE VARIATIONAL PROBLEM

In a narrow, elongated basin such as Knight Inlet, physical intuition might suggest that the Coriolis acceleration should not greatly affect the barotropic tidal flow. In practice, however, the inclusion of the Coriolis term produces certain difficulties, regardless of whether or not the dissipation term is retained. Following an outline of the problem and the method of solution, two questions will be discussed in this section; they are a) the specification of the condition at the open boundary, and b) the effect of a sudden change in depth.

Consider the simplest possible (i.e., linear, frictionless) equations of wave motion taking into account the Earth's rotation. In the notation of Chapter 2, with f denoting the Coriolis parameter, and $\underset{\sim}{e}_z$ a unit vertical vector directed upwards, the governing equations are

$$-i\omega\underset{\sim}{U} + f\underset{\sim}{e}_z \times \underset{\sim}{U} = -g\underset{\sim}{\nabla}H \tag{13}$$

$$-i\omega H + \underset{\sim}{\nabla} \cdot (D\underset{\sim}{U}) = 0 \quad . \tag{14}$$

Equation (13) can also be written as

$$\underset{\sim}{U} = \frac{g}{(\omega^2 - f^2)}(-i\omega\underset{\sim}{\nabla}H - f\underset{\sim}{e}_z \times \underset{\sim}{\nabla}H) \quad , \tag{15}$$

and the substitution of (15) into (14) yields

$$\underset{\sim}{\nabla} \cdot (D\underset{\sim}{\nabla}H) + \frac{(\omega^2 - f^2)}{g}H + i\frac{f}{\omega}\underset{\sim}{e}_z \cdot (\underset{\sim}{\nabla} \times D\underset{\sim}{\nabla}H) = 0 \quad . \tag{16}$$

The condition (8) of zero normal flow across the solid boundary becomes

$$(\underset{\sim}{n} \cdot \underset{\sim}{\nabla} + i\frac{f}{\omega}\,\underset{\sim}{\tau} \cdot \underset{\sim}{\nabla})H = 0 \text{ on } \Gamma_2 \quad , \tag{17}$$

where $\underset{\sim}{n}$ denotes the outward-directed normal unit vector and $\underset{\sim}{\tau} = \underset{\sim}{e}_z \times \underset{\sim}{n}$. Let us assume, for now, that we can specify the elevation at the open boundary, i.e.,

$$H \text{ given on } \Gamma_1 \quad . \tag{18}$$

Two approaches to the solution of (16), (17), and (18) have been considered; as in Chapter 2, both involve the separation of H into its real and imaginary parts, $H = h + is$, and an iterative scheme for the calculation of h and s. The third term of (16) and the second term of (17) are then "known" functions of space at each iterative step, for those terms contain only derivatives of s in the equation for h, and *vice versa*.

In the first approach, the "forcing" terms are simply carried along in the variational formulation. Therefore, the variational functional contains a boundary integral. For example, the problem statement for h, i.e.,

$$\underset{\sim}{\nabla} \cdot (D\underset{\sim}{\nabla}h) + \frac{(\omega^2 - f^2)}{g}h - \frac{f}{\omega}\,(D_x s_y - D_y s_x) = 0 \quad , \tag{19}$$

with

$$\frac{\partial h}{\partial n} - \frac{f}{\omega}\frac{\partial s}{\partial \tau} = 0 \quad \text{on } \Gamma_2 \quad , \tag{20}$$

and

$$h \text{ given on } \Gamma_1 \tag{21}$$

is equivalent to the variational condition $\delta J_1 = 0$ for all δh vanishing on Γ_1 with

$$J_1(h,h_x,h_y) = \int_A \left[\frac{D}{2}(h_x^2 + h_y^2) - \frac{(\omega^2 - f^2)}{2g} h^2 \right.$$

$$\left. + \frac{f}{\omega}(D_x s_y - D_y s_x)h \right] dA - \int_{\Gamma_2} \frac{fD}{\omega} \frac{\partial s}{\partial \tau} h \, d\xi \quad , \quad (22a)$$

where ξ denotes arc length along the contour. Similarly, the variational integral for s is given by

$$J_1(s,s_x,s_y) = \int_A \left[\frac{D}{2}(s_x^2 + s_y^2) - \frac{(\omega^2 - f^2)}{2g} s^2 \right.$$

$$\left. - \frac{f}{\omega}(D_x h_y - D_x h_y)s \right] dA + \int_{\Gamma_2} \frac{fD}{\omega} \frac{\partial h}{\partial \tau} s \, d\xi \quad . \quad (22b)$$

Obviously, this approach can also be implemented with the more general forcing functions that would result from the insertion of, say, a frictional term in the momentum equation. The forcing function might then also involve derivatives of the function that is varied, as was the case with the right-hand side considered in Chapter 2, and denoted by F_n in equation (12). The value of the function can then be computed from the results of the previous iteration.

In the alternative approach, the specific form of the forcing term is considered, and the boundary condition along Γ_2 is made a natural condition of a variational principle that consists only of an area integral. Consider again the problem for h. If we define

$$\underset{\sim}{\psi} = Ds_y \underset{\sim}{e}_x - Ds_x \underset{\sim}{e}_y \quad ,$$

equation (19) can be written as

$$\underset{\sim}{\nabla} \cdot (D \underset{\sim}{\nabla} h) + \frac{\omega^2 - f^2}{g} h - \frac{f}{\omega} \underset{\sim}{\nabla} \cdot \underset{\sim}{\psi} = 0 \quad ,$$

and a variational principle can be constructed in the usual way.

Let

$$-\delta J_2(h,h_x,h_y) = \iint_A \left[\underset{\sim}{\nabla} \cdot (D\underset{\sim}{\nabla} h) + \frac{\omega^2 - f^2}{g} h - \frac{f}{\omega} \underset{\sim}{\nabla} \cdot \underset{\sim}{\psi} \right] \delta h \, dA \quad ;$$

the first two terms yield, by a routine manipulation,

$$-\delta \int_A \frac{D}{2} |\underset{\sim}{\nabla} h|^2 dA + \oint_\Gamma D \frac{\partial h}{\partial n} \delta h \, d\xi + \delta \int_A \frac{(\omega^2 - f^2)}{2g} h^2 \, dA \quad .$$

Because $\underset{\sim}{\psi}$ is a function of s only, the third term is equal to

$$\delta \int_A \frac{f}{\omega} \underset{\sim}{\psi} \cdot \underset{\sim}{\nabla} h \, dA - \oint_\Gamma \frac{f}{\omega} \underset{\sim}{n} \cdot \underset{\sim}{\psi} \, \delta h \, d\xi \quad .$$

The integration of the boundary terms can be limited to Γ_2 since $\delta h \equiv 0$ on Γ_1, and, because

$$\underset{\sim}{n} \cdot \underset{\sim}{\psi} = D(s_y n_x - s_x n_y) = D \frac{\partial s}{\partial \tau} \quad ,$$

equation (20) is the natural boundary condition resulting from the variational condition

$\delta J_2 = 0$ for all δh vanishing on Γ_1 with

$$J_2(h,h_x,h_y) = \iint_A \left[\frac{D}{2}(h_x^2 + h_y^2) - \frac{(\omega^2 - f^2)}{2g} h^2 + \frac{fD}{\omega} (s_x h_y - s_y h_x) \right] dA \quad . \qquad (23a)$$

A similar derivation for s leads to

$$J_2(s,s_x,s_y) = \iint_A \left[\frac{D}{2}(s_x^2 + s_y^2) - \frac{(\omega^2 - f^2)}{2g} s^2 \right.$$

$$+ \frac{fD}{\omega} (s_x h_y - s_y h_x) \Big] dA \quad . \qquad (23b)$$

Equations (23) can also be derived directly from (22).

For Knight Inlet, both the solution of equations (22a-b) and that of equations (23a-b) were programmed. The integration of all the terms over each element, and, for equations (22), over each boundary segment can be performed exactly. Hence, as expected, the two approaches lead to identical results at each step of the iteration.

Although little is gained computationally by use of the second formulation, it has a somewhat unusual property. The two variational problems defined by (23a) and (23b) are coupled through the last term of each integral. Because these terms are identical, it is possible to formulate a unique variational principle equivalent to the pair of coupled real equations and boundary conditons, resulting from the splitting of the complex equations (16), (17), and (18). Such a principle was given by Pearson and Winter (1977) [their equation (31)] and also, in a different form, by Hamblin (1976). A simple way to construct the global functional $J(h,h_x,h_y,s,s_x,s_y)$ is to set

$$-2\delta J = \int_A \Big[(16)\delta H^* + (16)^* \delta H \Big] \, dA$$

$$- \int_{\Gamma_2} D \Big[(17)\delta H^* + (17)^* \delta H \Big] \, d\xi \quad ,$$

where the numbers (16,17) denote the left-hand side of the respective equations, and the asterisk a complex conjugate. After some algebra, J turns out to be real and given by

$$J = \int_A \left[\frac{D}{2} (h_x^2 + h_y^2 + s_x^2 + s_y^2) - \frac{1}{2} \frac{(\omega^2 - f^2)}{g} (h^2 + s^2) \right.$$

$$\left. + \frac{f}{\omega} D (s_x h_y - h_x s_y) \right] dA \quad . \qquad (24)$$

The details of the derivation are described in Appendix A. It is easily shown that in the absence of rotation the variational principle is simply Hamilton's principle applied to the linear shallow water wave problem, i.e., the variational functional J is proportional to the difference between total kinetic (T) and potential (V) energies. However, with $f \neq 0$, the physical principle expressed by (24) is not entirely clear, but J is definitely not proportional to either T + V, as claimed by Hamblin (1976, 1978), or T-V as in Hamilton's principle.

RESULTS

Figure 11 shows the main axes of the tidal ellipses obtained by solving the Kelvin wave equations (22a,b) with the condition that $h = s = \sqrt{2}$ m on Γ_1. There are three major differences between these results and those described in Chapter 3 and summarized in Figure 8:

a. the minor axes of the ellipses of the elements close to the open boundary are much larger than in the previous case,

b. the tidal ellipses are also much "fatter" in the sill area, and

c. the maximum speed over the sill is about 75% larger than the corresponding value obtained with $E = 1 \times 10^{-2}$ m sec^{-1}.

The first point is expanded upon in the following section, and a

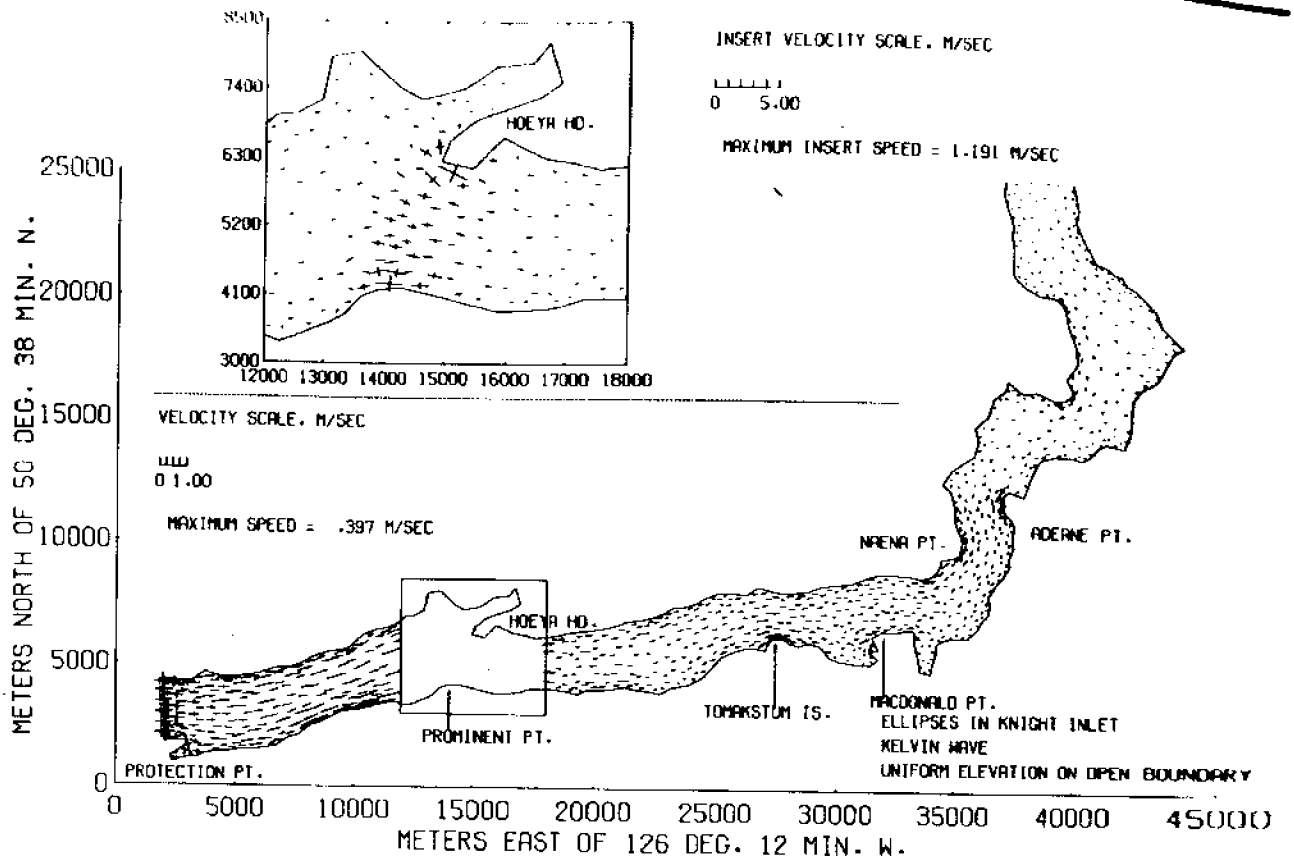

Figure 11. Axes of the tidal ellipses for the Kelvin wave problem when a uniform elevation is specified along the entrance of the fjord.

modification of the boundary condition at the entrance is proposed to eliminate what appears to be an unrealistic result. Both the second and third points appear to be related to the broad topic of the effects on waves of lateral boundaries. The rigorous mathematical description of such effects is very complex. A detailed catalog and comprehensive bibliography of various phenomena (e.g., partial or total reflection, trapping, diffraction and scattering, interactions) can be found in the recent book by LeBlond and Mysak (1978). Only a heuristic argument will be developed in this chapter, leading to the conjecture that Poincaré waves generated at the sill might be the source of significant observed and calculated cross-

channel motions in that area. The third point can be partly explained by the absence of the frictional effect along the boundaries in the results of Figure 11. Without the Coriolis term the maximum speed over the sill occurs in the middle of the channel for $E = 1 \times 10^{-2}$ m sec^{-1}; with $E = 0$, it occurs in a boundary element and is about 35% larger. In all cases, the velocities away from the solid boundary are nearly identical.

MODIFICATION OF THE CONDITION AT THE OPEN BOUNDARY

When a uniform elevation is imposed along the mouth of the estuary, the nearby velocity field is characterized by the presence of a large permanent "half-eddy," i.e., the direction of the flow at one end of Γ_1 is almost opposite to that at the other end as shown in Figure 12. Such a feature is unrealistic and the boundary condition chosen on Γ_1 is clearly inappropriate. Pearson and Winter (1977) encountered a similar problem in their computation of tidal flow in a semi-elliptical basin. They argue that the great sensitivity of the currents in the interior of the domain to small changes in the seaward boundary condition results from the fact that the mathematical problem is not well-posed. They discuss the implementation of a proper matching technique, the so-called "admittance condition" (e.g., Lee, 1971; Garrett, 1975). In actual practice, they advocate the use of a "simpler procedure in which a small phase gradient is imposed on the tidal height input at the seaward boundary." Such a procedure is essentially a trial-and-error approach, guided by the condition that the flow along Γ_1 should be nearly normal to the entrance of the basin. Maier-Reimer (1977) also reports "obviously falsified results" in the neighborhood of a

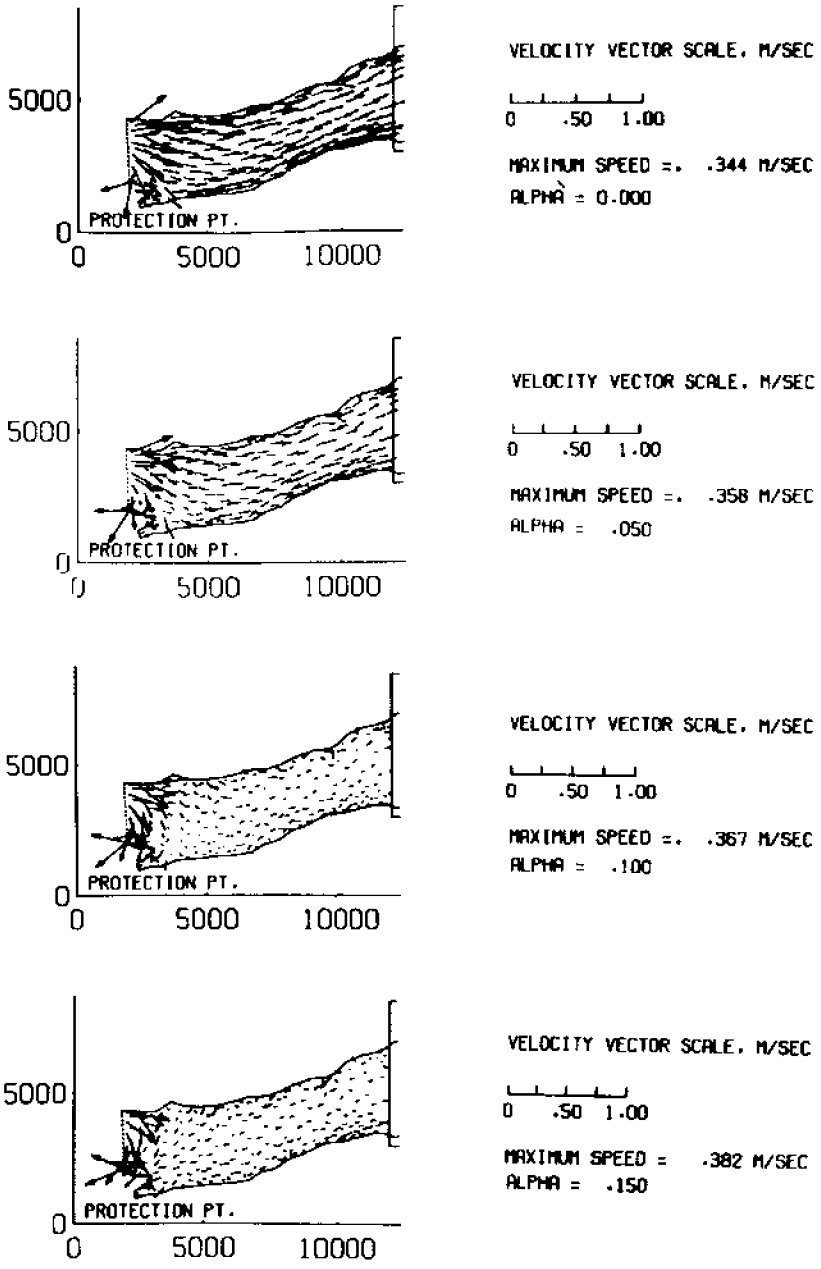

Figure 12. Successive patterns of the velocity vector field near the entrance when Coriolis acceleration is included and a uniform elevation imposed along the open boundary.

"doubtful boundary condition" in his model of the residual circulation in the North Sea; he attributes the feature to a lack of geostrophic adjustment along the boundary and chooses to ignore the problem on the basis of its limited spatial extent (4 to 6 grid lines).

In the case of Knight Inlet, the phenomenon is also restricted to a few elements adjacent to Γ_1 (Figures 11 and 12); it appears to be due to the inconsistency of the boundary conditions at the junctions of Γ_1 and Γ_2, and not related to the "effect of landward tidal reflection" (Pearson and Winter, 1977). Taylor's condition for total reflection of the incident Kelvin wave (Taylor, 1921, or see Defant, 1961, p. 213) is certainly satisfied for such a narrow channel; moreover, the Poincaré waves that are necessary to satisfy the condition of no normal flow at the head of the inlet decay within a few kilometers of the landward barrier. In order to make the boundary conditions consistent at their junctions, a transverse slope must be specified across Γ_1 on both the incoming and the outgoing Kelvin waves, or equivalently, a phase gradient. The appropriate modification can be estimated in several ways.

The first method (Taylor, 1919) follows directly from the assumption of cross-channel geostrophic balance along Γ_1, i.e., in the y-direction (see Figure 2). With $\underset{\sim}{U} = U\underset{\sim}{e}_x + V\underset{\sim}{e}_y$, such a balance is expressed by

$$\frac{\partial H}{\partial y} = -\frac{f}{g} U \quad . \tag{25}$$

With $V = 0$, the longitudinal velocity near Γ_1 is given by $U = -i \frac{g}{\omega} \frac{\partial H}{\partial x}$, and it is easily verified that the boundary condition at the corners between Γ_1 and Γ_2 is uniquely defined. The velocity U can be estimated from the results obtained in the previous chapter with $E = 0$. In that case and with $h = s = \sqrt{2}$ m on Γ_1, the average value of U, over all elements that have at least one node on Γ_1, is $U = 14.2\ (1-i)$ cm $\sec^{-1}$ and (25) yields

$$\frac{\partial H}{\partial y} = -1.61 \times 10^{-6}(1-i) \quad . \tag{26}$$

A second estimate of the correct boundary condition can be derived from available analytical solutions for the problem of the reflection of a Kelvin wave by the end wall of a rectangular basin. For Knight Inlet, the most appropriate formula is the limit derived by Brown (1973) for very narrow canals. Consider a semi-infinite rotating canal of constant depth D that occupies the region defined by $x \geq 0$, $0 \leq y \leq a$, and define $c_o = (gD)^{\frac{1}{2}}$, $\theta = \frac{\omega a}{c_o}$, and $F = \frac{f}{\omega}$. Brown shows that if $\theta << 1$, the end effect is virtually absent [in fact, it is $O(\theta^2)$] and the elevation is approximately given by

$$\zeta = \mathrm{Re}\left[e^{-i\omega t} \left[(2-F\theta) \cos \theta X + i\theta F(1-2Y) \sin \theta X\right] \right] \quad , \tag{27}$$

where $X = \frac{x}{a}$ and $Y = \frac{y}{a}$. From (27), we see that the amplitude of H is independent of y to order θ^2. The phase of the elevation is symmetric about the mid-channel axis and negative on the right-hand side of the incoming wave; the phase difference between Y = 0 and Y = 1 is given by

$$\delta\phi = 2 \tan^{-1}\left(\frac{\theta F}{2-\theta F} \tan \theta X \right) \quad . \tag{28}$$

For the M_2 tide in Knight Inlet, with a = 3000 m and using a depth D = 200 m representative of the outer basin, we have $\theta \simeq 9.5 \times 10^{-3}$ and $F \simeq 0.80$. Since $X \leq 33$, equation (28) can be approximated by

$$\delta\Phi \simeq \theta^2 FX = \frac{\omega f a x}{gD} \quad . \tag{29}$$

For x = 100 km, equation (28) yields $\delta\Phi = 0.143^o$ while (29) gives $\delta\Phi \simeq 0.136^o$. This approach is useful because it gives some indication of the magnitude of the phase gradient that is appropriate

across Γ_1. However, its applicability to a long fjord such as Knight Inlet is restricted mainly by the assumption of constant depth. This is also true of the results of Pearson (1977).

A third approach (M. Rattray, Jr., personal communication) is based on the limited extent of the perturbation due to a poor choice of the mouth condition and the apparent adjustment that occurs between Γ_1 and the sill (Figure 11). The finite element grid could be extended seaward of Γ_1 in a fictitious rectangular canal at the end of which a uniform elevation would be specified; the solution at Γ_1 would then have adjusted to geostrophy and the flow would be normal to the true entrance as desired.

The fourth approach is somewhat more general and yet fairly easy to implement on a computer. It consists of specifying the surface elevation at only one point of the open boundary and the direction of the velocity along the entire entrance. This strategy has also been used by Walters and Cheng (1978), although for a completely different reason, namely, to satisfy better the requirement of continuity. Given the geometrical configuration of Knight Inlet, it seems reasonable to require that the velocity be normal to the entrance of the inlet segment. The boundary condition (18) is then replaced by

$$\underset{\sim}{U} \cdot \underset{\sim}{\tau} = 0 \quad \text{on } \Gamma_1 \quad , \tag{30}$$

or, upon substitution of (15), by

$$\frac{\partial H}{\partial n} + i \frac{\omega}{f} \frac{\partial H}{\partial \tau} = 0 \quad \text{on } \Gamma_1 \quad , \tag{31}$$

with H specified at one point of Γ_1. The new complex condition (31)

can again be incorporated in a pair of variational principles to be solved iteratively; for the real part of H, the variational functional becomes (see Appendix A)

$$J_3(h,h_x,h_y) = \int_A \left[\frac{D}{2}(h_x^2 + h_y^2) - \frac{(\omega^2 - f^2)}{2g} h^2 \right.$$

$$\left. + \frac{fD}{\omega} (s_x h_y - s_y h_x) \right] dA - \int_{\Gamma_1} D \frac{(\omega^2 - f^2)}{\omega f} \frac{\partial s}{\partial \tau} h \, d\xi \quad , \qquad (32a)$$

while the imaginary part, s, is given by $\delta J_3 = 0$ with

$$J_3(s,s_x,s_y) = \int_A \left[\frac{D}{2}(s_x^2 + s_y^2) - \frac{(\omega^2 - f^2)}{2g} s^2 \right.$$

$$\left. + \frac{fD}{\omega} (s_x h_y - s_y h_x) \right] dA + \int_{\Gamma_1} D \frac{(\omega^2 - f^2)}{\omega f} \frac{\partial h}{\partial \tau} s \, d\xi \quad . \qquad (32b)$$

In the finite element solution of equations (32), the variations δh and δs vanish at only one node on the open boundary. The results obtained with $h = s = \sqrt{2}$ m at the central node of Γ_1 are shown in Figure 13. The tidal ellipses in the neighborhood of the entrance are almost straight lines and the velocities are almost in phase on both sides of Γ_1. This is illustrated by the velocity vector field at $\alpha = 0$ shown in Figure 14. The calculated cross-channel slopes of h and s are $-(1.68 \pm 0.12) \times 10^{-6}$ and $(1.55 \pm 0.12) \times 10^{-6}$ respectively, very close to the values predicted by equation (26). The uncertainty affecting the computed results is determined from the convergence criterion (see "Numerical Considerations") applied to the iterative procedure; a tolerance of 10^{-4} was used in these calculations and convergence was achieved after 13 iterations. The phase difference across Γ_1 is found equal to $(0.155^\circ \pm 0.011^\circ)$ and is comparable with the result of equation (28). The phase relative to that at the

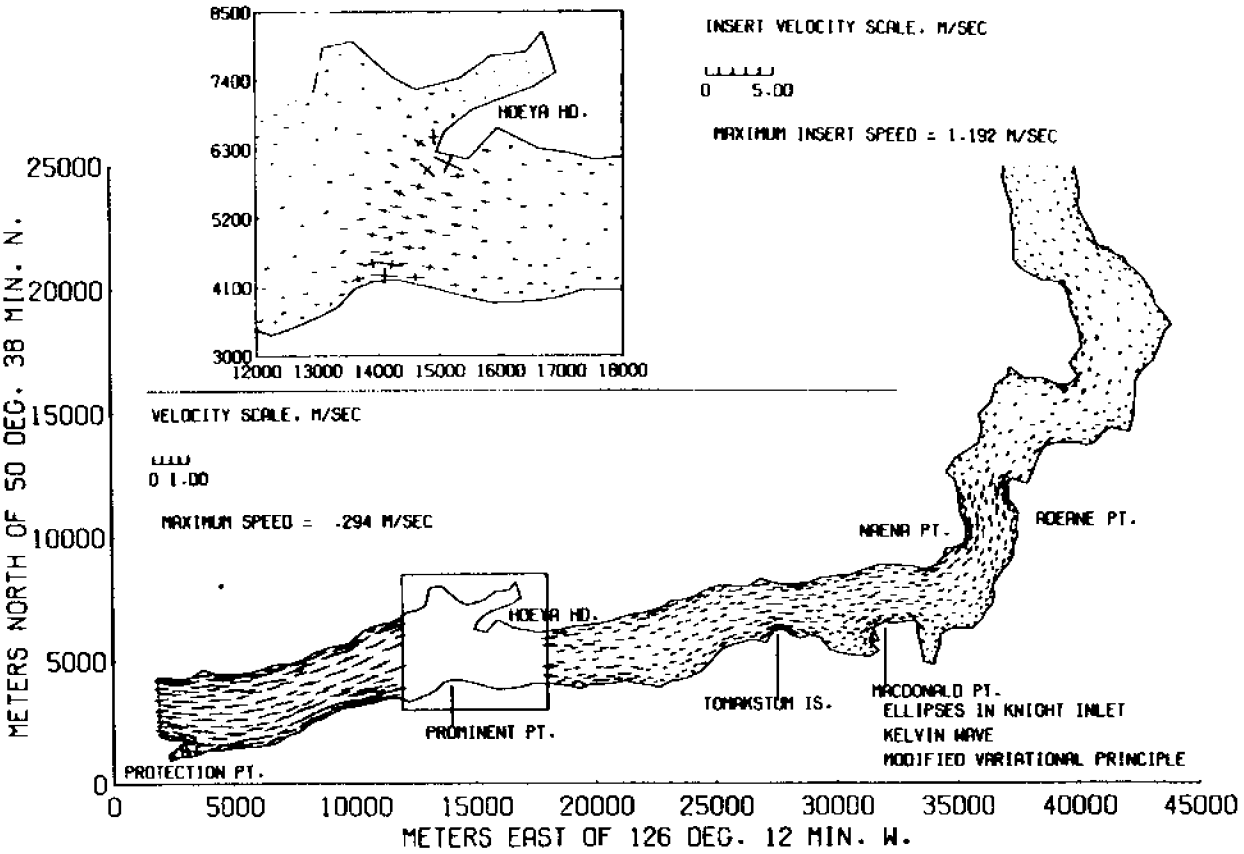

Figure 13. Axes of the tidal ellipses for the Kelvin wave problem when the tangential velocity is required to vanish along the open boundary and the tidal height specified only at the central node of that boundary.

central node is negative at the southern shore, positive on the other side.

An independent estimate of the phase difference between the two sides of the channel is available from tide gauge measurements made on both sides of station 3 (see Figure 1). After correction for clock drifts (a few seconds at most), the mean of four observations is 0.13^{o} (≈16 seconds) with a standard deviation of 0.017^{o} (Freeland, personal communication). From the r.m.s. noise level in similar tidal elevation spectra, Freeland and Farmer (1980) evaluate an expected error in phase determination of 0.08^{o} at the M_2 frequency.

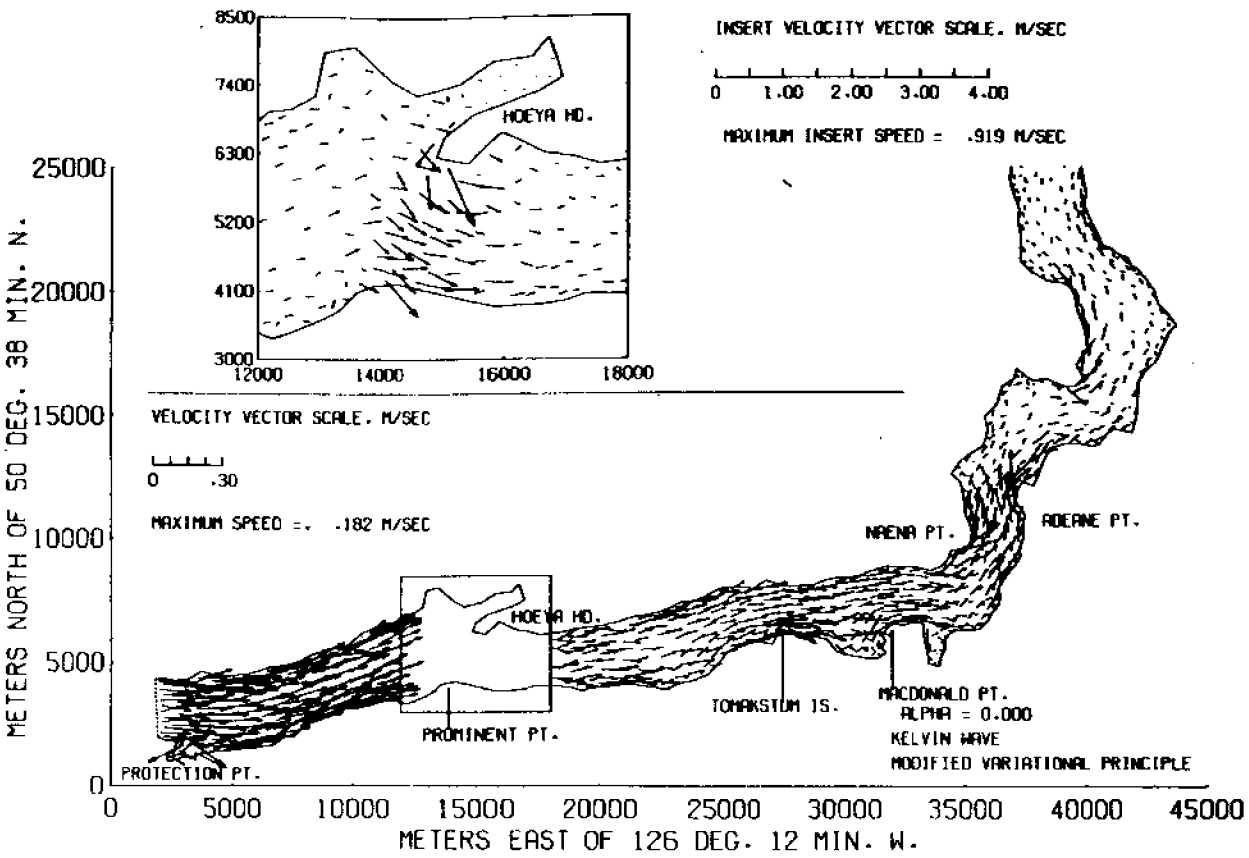

Figure 14. Velocity vector field for the Kelvin wave problem at α = 0, i.e., near the time of maximum flood currents at the entrance; the boundary condition is the same as in Figure 13.

However, they argue that such error bars should be regarded as pessimistic estimates considering the consistency in sign of many observations of very small phase differences. Although the size of the sample described above is very small, the magnitude of the standard deviation tends to add credibility to the significance of the mean (using Student's *t*-test, the 95% confidence interval is $\pm 0.05^{\circ}$).

In conclusion, the general agreement amongst the several phase gradient estimates is very good and is unlikely to be fortuitous. The problem formulation described by equations (32) does provide a

means to eliminate the spurious eddy in the vicinity of the open boundary. A comparison of Figures 11 and 13 shows that the results over most of the inlet are not affected by the modification of the boundary condition.

EFFECTS OF THE SILL

As discussed in Chapter 3, a major effect of the sill is a sudden and large increase in the magnitude of the longitudinal velocity in order to satisfy mass continuity. This effect is also observed when the Coriolis term is included in the equations, and the resulting longitudinal distribution of the amplitude of the elevation is similar to that of Figure 7a. However, the amplification factor between Siwash Bay and Γ_1 is a bit smaller than in the absence of rotation (1.0310 instead of 1.0351) and therefore closer to the observed value (see "Comparison with Available Data"). The amplitude ratio between Wahshihlas Bay and Siwash Bay is almost unchanged (1.0129).

A second effect of the sill is a perturbation of the geostrophic adjustment in the cross-channel direction that was achieved in the neighborhood of the entrance by the method just described. For the linear case under study, with $\underset{\sim}{U} = U\underset{\sim}{e}_x + V\underset{\sim}{e}_y$, a consideration of the momentum equation in the y-direction indicates that the two terms that can balance the increase of "f U" are:

i) the force due to lateral pressure gradient, "$g \frac{\partial H}{\partial y}$"

ii) a cross-channel acceleration, "$-i\omega V$."

It appears that both terms are needed to explain the results obtained here. Constraints on the problem are 1) the condition of zero normal flow at the lateral boundaries, and 2) the requirement that the free-surface elevation and the transport be continuous

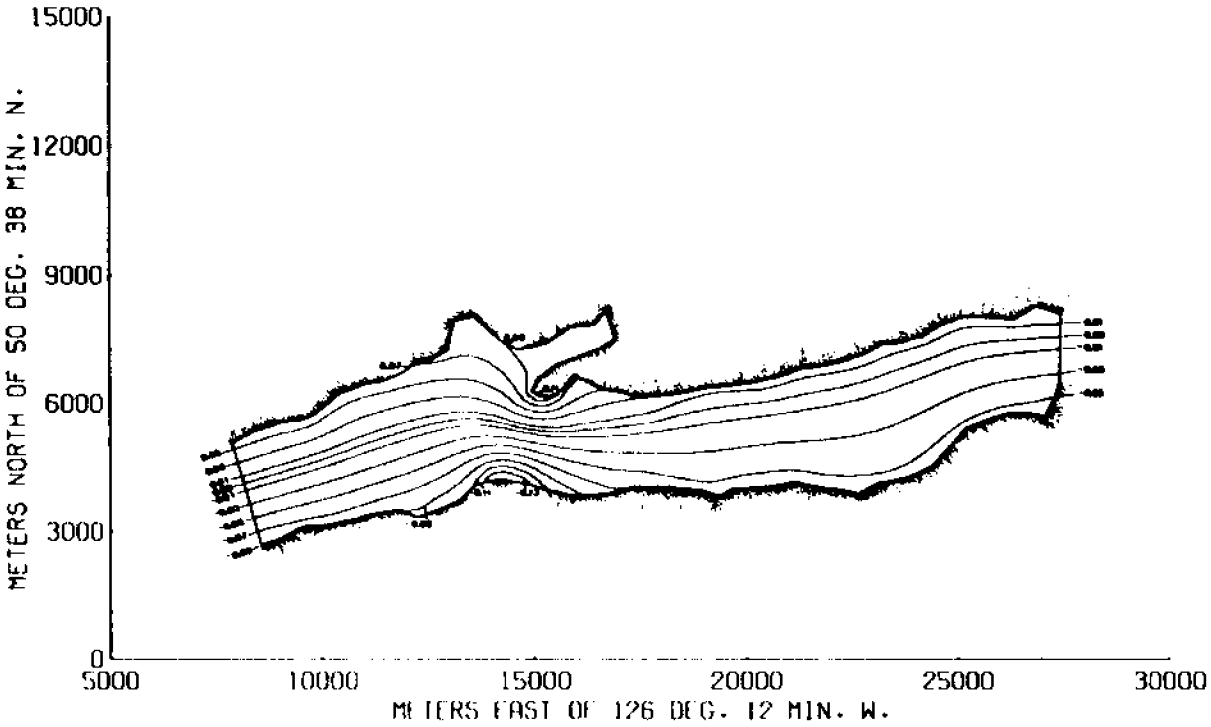

Figure 15. Phase lines on the refined grid for the Kelvin wave problem.

over the obstacle.

The cross-channel variation in the calculated free-surface elevation is best shown by the results for the phase. Figure 15 displays the phase relative to the central node of Γ_1 as calculated on the refined grid. Across the western open boundary of the refined grid, the cross-channel phase difference $\delta\Phi$ is 0.152°, very close to the corresponding value across Γ_1, the open boundary of the coarser grid. In the vicinity of the sill, $\delta\Phi$ increases rapidly to a maximum of about 0.25°, indicating an increased tilting of the free surface in the shallower region. No field evidence is available to verify or contradict this observation based on calculations. However, the result is not inconsistent with the phase difference obtained by applying locally the equation derived from Brown's (1973) results for a constant depth, narrow,

rectangular channel. With x = 75 km and D = 50 m as the average depth at the sill, equation (28) yields $\delta\Phi = 0.37^{o}$ (this equation, however, is rather sensitive to the choice of mean depth and with D = 75 m, for example, it gives $\delta\Phi \approx 0.25^{o}$). Figure 15 clearly shows the tendency towards geostrophic adjustment by increased tilting of the sea surface. However, the tidal ellipses of Figure 13 also indicate significant cross-channel motion at the M_2 frequency in the vicinity of the sill.

In order to satisfy the boundary condition at the lateral walls, the cross-channel motion must be composed of Poincaré modes, i.e., the solution is oscillatory in the "y-direction." Since $\frac{\pi^2}{a^2} - \frac{(\omega^2 - f^2)}{gD} > 0$, none of these Poincaré waves propagates away from the sill, and the "x-dependence" is an exponential decay on both sides of the obstacle. The evidence for the presence of those modes in the results of the calculations is somewhat vague for several reasons. First, the bathymetry of the inlet and the configuration of the shoreline are sufficiently complex to blur the idealized picture of "pure" Poincaré waves generated and trapped at a step-like obstacle in a straight channel. Second, the finite element grids used in this study are only marginally suitable to resolve perturbations of the basic flow on such small scales. Third, the limitation imposed on the accuracy of the solution by the finite rate of convergence of the iterative scheme has to be kept in mind. Last, the condition of zero normal transport along the solid boundary is not as well satisfied as in the absence of rotation, especially in the proximity of sharp angles (see Figures 13 and 14, near Hoeya Head and MacDonald Point for instance). The refinement of the grid does not eliminate the problem. It may be that

the boundary condition needs to be more strictly enforced than is, in some cases, the natural boundary condition of a variational principle. A procedure to that effect has been suggested recently (Jamart, 1980), but it has not been implemented for Knight Inlet. In support of the proposed conjecture, note that in the center of the channel the ratio of the length of the minor axis to that of the major axis is about 0.30 over the sill and decays rapidly on both sides, somewhat faster on the wider, down-inlet side of the sill than in the up-inlet direction. Short wavelength oscillations can be seen in plots of cross-channel distribution of the Fourier coefficients of the north-south velocity, but the confidence limits are fairly large. Finally, a comparison of Figures 5 and 14 shows that the pattern of velocity directions is less smooth when the Coriolis term is included in the calculations. Observations also provide evidence of cross-channel motion at tidal frequency.

The velocity measurements of Pickard and Rodgers (1959) at stations 3½ and 5 (Figure 1) clearly show that large transverse components of current are observed in Knight Inlet. The cross-channel currents are much larger at the sill than in deep water. Moreover, Pickard and Rodgers point out that "the directions and magnitudes (of these cross-channel currents) appear to vary randomly and do not show any significant tidal component" at station 5, whereas, at the sill station, there is "some apparent tidal periodicity in the transverse components." They attribute this latter feature "to an effect of the bottom topography which apparently results in the flood and ebb direction being less than 180^{o} apart in that inlet section." In fact, their interpretation (see Pickard and Rodgers, 1959, pp. 668-669) is based solely on the configuration of the

shoreline, and hence differs from the present suggestion that the sill is responsible for the generation of transverse waves in the inlet. Further observational evidence for transverse motion at tidal frequencies can be deduced from Cannon's current measurements at stations 4, 5_N, and 5_S. Table 2 lists the magnitudes and phases of the M_2 spectral components communicated by G. Cannon, and the ellipses' characteristics that were calculated from those data. As discussed in "Comparison with Available Data," the large phase differences between observations at different depths on a given mooring are indicative of the importance of baroclinic motion in the inlet. Nevertheless, it appears that significant transverse currents are measured at the station closest to the sill while all North-South velocity components recorded at stations 5_N and 5_S are below the noise level of the spectra.

Table 2: Results of current measurements at stations 4, 5_N, and 5_S (communicated by G. Cannon).

M_2 TIDAL Currents

		EASTWARD VELOCITY		NORTHWARD VELOCITY		TIDAL ELLIPSES		
STATION NUMBER	Depth (m)	SPEED ($cm\ sec^{-1}$)	PHASE† (degree)	SPEED ($cm\ sec^{-1}$)	PHASE† (degree)	SEMI-MAJOR AXIS ($cm\ sec^{-1}$)	SEMI-MINOR AXIS†† ($cm\ sec^{-1}$)	ORIENTATION (counter clockwise from East) (degree)
4	65	8.32	163.06	3.51	-132.21	8.48	3.12	11.86
4	125	7.90	125.96	1.65	-108.58	7.96	1.34	-7.07
4	300	5.69	77.21	1.97	-31.86	5.53	-1.85	-7.53
4	363	7.50	21.70	2.47	-61.25	7.51	-2.46	2.61
5_N	75	10.28	112.11	0.49	-12.30	10.28	-0.41	-1.53
5_N	294	8.74	145.00	0.86	124.18	8.78	-0.31	5.24
5_S	82	13.28	112.68	1.09	-49.87	13.32	-0.33	-4.47
5_S	323	6.42	143.75	0.59	-56.25	6.45	0.20	-4.95

† Relative to an arbitrary time origin (the beginning of the record).

†† A minus sign indicates clockwise rotation of the velocity vector.

5 SUMMARY, CONCLUSIONS, AND RECOMMENDATIONS FOR FUTURE WORK

For tidal computations, the solution of the shallow water wave equations in Fourier space or in terms of harmonic constituents is an attractive alternative to the conventional time-stepping methods. The harmonic approach has proved useful in the computation of tides in ocean basins (Hendershott, 1977), shallow bays (Synder *et al.*, 1979), harbors (Kawahara and Hasegawa, 1978), and deep inlets (the present study). The premise of the approach -- the decomposability of the time-dependent tidal signal into modes corresponding to discrete frequencies -- is also commonly used to verify physical or numerical models (e.g., Whalin *et al.*, 1976, Ronday, 1979).

The procedure proposed by Pearson and Winter (1977) for the computation of tidal constituents and the simpler linear version described by Jamart and Winter (1978) are outlined in Chapter 2.

Chapter 3 describes the application to Knight Inlet, British Columbia, of the simplified version of the computational procedure. It is assumed that the internal mechanisms that extract energy from the barotropic tidal flow in the vicinity of the sill can be modeled as a body force proportional to the velocity divided by the local time-mean depth. Such a dissipation term is most influential over the sill and along the shores of the fjord. Bottom friction in the usual sense is assumed negligible, as is the Coriolis acceleration in the first part of the study. The advective terms are also presumed of secondary importance in the calculation of the dominant (M_2) tidal constituent. After elimination of the velocity, the

equations and boundary conditions governing the spatial distribution of the elevation are rephrased in terms of a variational problem that is solved by means of a finite element method. The (constant) dissipation coefficient is adjusted so that the calculated phase of the tidal elevation matches observations at three stations along the inlet. The amplitude of the elevation and the magnitude and phase of the longitudinal velocity are found to be in good agreement with all of the available data. The conclusion is that the simple linearized model adequately reproduces the main features of the dominant tidal constituent in a deep estuary such as Knight Inlet.

A variational principle can also be constructed for the Kelvin wave problem considered in Chapter 4, i.e., the case where the Coriolis term is inserted in the momentum equation and the dissipation term neglected. It is important that boundary conditions of different types be consistent at the junctions of the boundary segments along which they are prescribed. Specifically, when rotation is taken into account, the specification of the tidal height along the open boundary should include a phase gradient which appropriately reflects lateral dynamics in order to eliminate a spurious "half-eddy" across the mouth of the inlet. Several ways of estimating this *a priori* unknown phase gradient are discussed. The most general procedure appears to be a reformulation of the boundary condition at the estuary mouth, which consists of specifying the surface elevation at only one point of the open boundary and the direction of the velocity along the entire entrance. Given the geometrical configuration of Knight Inlet, it seems reasonable to require that the velocity be normal to the entrance of the fjord. This condition can be incorporated in the variational formulation of the Kelvin

wave problem. The cross-channel phase difference calculated by implementing this strategy is consistent with other estimates and with the value measured at a nearby location. Future work along these lines could include the consideration of more general boundary conditions (e.g., spatially and/or time-varying flow direction, complete specification of velocity) and the restoration of the dissipation term in the momentum equation. A deep and narrow fjord such as Knight Inlet does not appear to be an appropriate case on which to carry out such developments.

At the end of Chapter 4, it is conjectured that the cross-channel motions of tidal frequency that are observed in the vicinity of the sill may be a manifestation of trapped Poincaré waves generated at the sill. If this speculation is valid, such a process should be relevant to the study of lateral mixing in fjords. In any event, the phenomenon deserves further investigation; for a theoretical study, a more schematized geometry (rectangular channel, single step perpendicular to the longitudinal axis) would be most appropriate.

APPENDIX A DERIVATION OF THE VARIATIONAL PRINCIPLES FOR THE KELVIN WAVE PROBLEM

1. Conventional boundary condition

After elimination of the velocity, the spatial distribution of the free-surface elevation, H, is governed by equations (16) to (18) of Chapter 4. These equations are

$$\underset{\sim}{\nabla} \cdot D\underset{\sim}{\nabla}H + \frac{(\omega^2 - f^2)}{g} H + i\frac{f}{\omega} \underset{\sim}{e}_z \cdot (\underset{\sim}{\nabla} \times D\underset{\sim}{\nabla}H) = 0 \text{ in } A \quad (A\text{-}1)$$

$$\text{with } H \text{ given on } \Gamma_1, \quad (A\text{-}2)$$

$$\text{and } \frac{\partial H}{\partial n} + i\frac{f}{\omega}\frac{\partial H}{\partial \tau} = 0 \quad \text{on } \Gamma_2. \quad (A\text{-}3)$$

To construct a variational principle equivalent to (A-1,2,3), set

$$-2\delta J = \int_A [(A\text{-}1)\delta H^* + (A\text{-}1)^*\delta H]\, dA$$

$$- \int_{\Gamma_2} D[(A\text{-}3)\delta H^* + (A\text{-}3)^*\delta H]\, d\xi \quad , \quad (A\text{-}4)$$

where the asterisk denotes a complex conjugate and the equation numbers stand for the left-hand sides of the equations. In view of (A-2), one has

$$\delta H = \delta H^* = 0 \quad \text{on } \Gamma_1. \quad (A\text{-}5)$$

Consider each term of (A-4) separately. The first term can be transformed as follows:

$$\int_A (\underset{\sim}{\nabla} \cdot D\underset{\sim}{\nabla}H)\delta H^*\, dA = \int_A \underset{\sim}{\nabla} \cdot (D\underset{\sim}{\nabla}H\delta H^*)\, dA - \int_A D\underset{\sim}{\nabla}H \cdot \underset{\sim}{\nabla}\delta H^*\, dA$$

$$= \oint_{\Gamma} D \frac{\partial H}{\partial n} \delta H^* \, d\xi - \int_A D \underset{\sim}{\nabla} H \cdot \delta \underset{\sim}{\nabla} H^* \, dA. \qquad \text{(A-6)}$$

Similarly, the complex conjugate of that term is equal to

$$\oint_{\Gamma} D \frac{\partial H^*}{\partial n} \delta H \, d\xi - \int_A D \underset{\sim}{\nabla} H^* \cdot \delta \underset{\sim}{\nabla} H \, dA. \qquad \text{(A-7)}$$

The second term and its conjugate yield

$$\int_A \frac{(\omega^2 - f^2)}{g} (H \delta H^* + H^* \delta H) \, dA - \delta \int_A \frac{(\omega^2 - f^2)}{g} H H^* \, dA. \qquad \text{(A-8)}$$

The third term of (A-4) and its conjugate are

$$\int_A i \frac{f}{\omega} \left[\underset{\sim}{e}_z \cdot (\underset{\sim}{\nabla} \times D \underset{\sim}{\nabla} H) \delta H^* - \underset{\sim}{e}_z \cdot (\underset{\sim}{\nabla} \times D \underset{\sim}{\nabla} H^*) \, \delta H \right] dA. \qquad \text{(A-9)}$$

Because of (A-5), the contour of the boundary integral in (A-4) can be replaced by the complete perimeter of the domain. The terms involving the normal derivative and its conjugate are simply

$$- \oint_{\Gamma} D \left(\frac{\partial H}{\partial n} \delta H^* + \frac{\partial H}{\partial n} \delta H \right) d\xi \qquad \text{(A-10)}$$

and they cancel the boundary integrals of (A-6) and (A-7). The remaining term is successively equal to

$$- \oint_{\Gamma} i \frac{f}{\omega} D \frac{\partial H}{\partial \tau} \delta H^* \, d\xi = -\underset{\sim}{e}_z \cdot \oint_{\Gamma} i \frac{f}{\omega} \underset{\sim}{n} \times D \underset{\sim}{\nabla} H \, \delta H^* \, d\xi$$

$$= -\underset{\sim}{e}_z \cdot \int_A i \frac{f}{\omega} \underset{\sim}{\nabla} \times (D\underset{\sim}{\nabla}H \, \delta H^*) \, dA$$

$$= -\int_A i \frac{f}{\omega} \underset{\sim}{e}_z \cdot (\underset{\sim}{\nabla} \times D\underset{\sim}{\nabla}H) \, \delta H^* \, dA$$

$$+ \int_A i \frac{f}{\omega} \underset{\sim}{e}_z \cdot (D\underset{\sim}{\nabla}H \times \underset{\sim}{\nabla}\delta H^*) \, dA. \quad \text{(A-11)}$$

the first term of (A-11) and its conjugate cancel (A-9); the second term and its conjugate yield

$$\int_A i \frac{f}{\omega} D\underset{\sim}{e}_z \cdot (\underset{\sim}{\nabla}H \times \delta\underset{\sim}{\nabla}H^* - \underset{\sim}{\nabla}H^* \times \delta\underset{\sim}{\nabla}H) \, dA$$

$$= \int_A i \frac{f}{\omega} D\underset{\sim}{e}_z \cdot (\underset{\sim}{\nabla}H \times \delta\underset{\sim}{\nabla}H^* + \delta\underset{\sim}{\nabla}H \times \underset{\sim}{\nabla}H^*) \, dA$$

$$= \delta \int_A i \frac{f}{\omega} D\underset{\sim}{e}_z \cdot (\underset{\sim}{\nabla}H \times \underset{\sim}{\nabla}H^*) \quad . \qquad \text{(A-12)}$$

Summing the contributions (A-6) to (A-12), one obtains

$$-2\,\delta J = \delta \int_A \left[-D\underset{\sim}{\nabla}H \cdot \underset{\sim}{\nabla}H^* + \frac{(\omega^2 - f^2)}{g} HH^* \right.$$

$$\left. + i \frac{f}{\omega} D\underset{\sim}{e}_z \cdot (\underset{\sim}{\nabla}H \times \underset{\sim}{\nabla}H^*) \right] dA \quad .$$

Upon substitution of $H = h + is$, equation (A-13) leads to equation (24), i.e.,

$$J = \int_A \left[\frac{D}{2} (h_x^2 + h_y^2 + s_x^2 + s_y^2) - \frac{(\omega^2 - f^2)}{2g} (h^2 + s^2) \right.$$

$$\left. + \frac{f}{\omega} D \, (s_x h_y - h_x s_y) \right] dA \quad . \qquad \text{(A-14)}$$

2. Modified boundary condition

Consider now the problem defined by equations (16), (17), and (31) of Chapter 4, i.e., (A-1), (A-3) and

$$\frac{\partial H}{\partial n} + i\,\frac{\omega}{f}\,\frac{\partial H}{\partial \tau} = 0 \text{ on } \Gamma_1,$$

with H specified at one point on Γ_1. (A-15)

An additional boundary integral should be added to equation (A-4), which becomes

$$-2\delta J = \int_A [(A\text{-}1)\delta H^* + (A\text{-}1)^*\delta H]\ dA - \int_{\Gamma_2} D[(A\text{-}3)\delta H^* + (A\text{-}3)^*\delta H]\ d\xi - \int_{\Gamma_1} D[(A\text{-}15)\delta H^* + (A\text{-}15)^*\delta H]\ d\xi \quad . \tag{A-16}$$

The area integral is again equal to the sum of (A-6) to (A-9). The two contour integrals can be combined to yield

$$(A\text{-}10) + (A\text{-}11) - \int_{\Gamma_1}\left(i\ D\ \frac{(\omega^2 - f^2)}{\omega f}\right)\left(\frac{\partial H}{\partial \tau}\delta H^* - \frac{\partial H^*}{\partial \tau}\ \delta H\right)\ d\xi \quad . \tag{A-17}$$

The final expression corresponding to (A-13) becomes

$$-2\delta J = \delta \int_A \left[-D(h_x^2 + h_y^2 + s_x^2 + s_y^2) + \frac{(\omega^2 - f^2)}{g}\ (h^2 + s^2) - 2\ \frac{fD}{\omega}\ (s_x h_y - h_x s_y)\right] dA + \int_{\Gamma_1}\left(2D\frac{(\omega^2 - f^2)}{\omega f}\right)\left(\frac{\partial s}{\partial \tau}\ \delta h - \frac{\partial h}{\partial \tau}\ \delta s\right) d\xi \quad , \tag{A-18}$$

and leads directly to equation (32) of Chapter 4.

REFERENCES

Brebbia, C.A., and P.W. Partridge, 1976. Finite element simulation of water circulation in the North Sea. Applied Mathematical Modelling, *1*(2): 101-107.

Brettschneider, G., 1967. Anwendung des hydrodynamisch-numerischen Verfahrens zur Ermittlung der M_2--Mitschwingungsgezeit in der Nordsee. Mitteilungen des Instituts für Meerskunde der Universität Hamburg, VII.

Brown, P.J., 1973. Kelvin-wave reflection in a semi-infinite canal, Journal of Marine Research, *31*(1): 1-10.

Connor, J.J., and J.D. Wang, 1973. Mathematical models of the Massachusetts Bay, Part I: Finite element modeling of two-dimensional hydrodynamic circulation. Report No. MITSG 74-4, Massachusetts Institute of Technology, Cambridge, Massachusetts, 57 pp.

Connor, J.J., and J.D. Wang, 1974. Finite element modelling of hydrodynamic circulation. *In*: Numerical Methods in Fluid Dynamics, C.A. Brebbia and J.J. Connor [Eds.],pp. 355-387. Pentech Press, London.

Crean, P.B., 1978. A numerical model of barotropic mixed tides between Vancouver Island and the mainland and its relation to studies of the estuarine circulation. *In*: Hydrodynamics of Estuaries and Fjords, J.C.J. Nihoul [Ed.], Elsevier Oceanography Series, *23*, pp. 283-313. Elsevier Scientific Publishing Company, Amsterdam.

Darwin, G.H., 1898. The Tides; and Kindred Phenomena in the Solar System. Reissued in 1962 by W.H. Freeman and Company, San Francisco, 378 pp.

Defant, A., 1961. Physical Oceanography, Vol. II. Pergamon Press, New York, 598 pp.

Dronkers, J.J., 1964. Tidal Computations in Rivers and Coastal Waters. North-Holland Publishing Company, Amsterdam, 518 pp.

Farmer, D.M., and J.D. Smith, 1978. Nonlinear internal waves in a fjord. *In*: Hydrodynamics of Estuaries and Fjords, J.C.J. Nihoul [Ed.], Elsevier Oceanography Series, *23*, pp. 465-493. Elsevier Scientific Publishing Company, Amsterdam.

Freeland, H.J., and D.M. Farmer, 1980. The circulation and energetics of a deep, strongly stratified fjord. Canadian Journal of Fisheries and Aquatic Sciences (in press).

Garrett, C., 1975. Tides in gulfs. Deep-Sea Research, *22*: 23-35.

Gray, W.G., 1977. An efficient finite element scheme for two-dimensional surface computations. *In*: Finite Elements in Water Resources, W.G. Gray, G.F. Pinder, and C.A. Brebbia [Eds.], pp. 4.33-4.49. Pentech Press, London.

Grotkop, G., 1973. Finite element analysis of long-period water waves. Computer Methods in Applied Mechanics and Engineering, *2*: 147-157.

Hamblin, P.F., 1976. Seiches, circulation, and storm surges of an ice-free Lake Winnipeg. Journal of the Fisheries Research Board of Canada, *33*: 2377-2391.

Hamblin, P.F., 1978. Finite element methods applied to the modelling of the circulation, seiches, tides, and storm surges in large lakes. *In*: Finite Elements in Fluids, Vol. 3, R.H. Gallagher, O.C. Zienkiewicz, J.T. Oden, M. Morandi Cecchi, and C. Taylor [Eds.], pp. 269-281. Wiley-Interscience, London.

Hansen, W., 1956. Theorie zur Errechnung des Wasserstandes und der Strömungen in Randmeeren nebst Anwendungen. Tellus, *8*(3): 287-300.

Heaps, N.S., 1969. A two-dimensional numerical sea model. Philosophical Transactions of the Royal Society of London, A, *220*: 93-137.

Hendershott, M.C., 1977. Numerical models of ocean tides. *In*: The Sea, Vol. VI, E.D. Goldberg, I.N. McCave, J.J. O'Brien, and J.H. Steele [Eds.], pp. 47-95. Wiley-Interscience, London.

Jamart, B.M., 1980. Finite element computation of barotropic tidal motions in deep estuaries. Ph.D. dissertation, University of Washington, Seattle, Washington.

Jamart, B.M., and D.F. Winter, 1978. A new approach to the computation of tidal motions in estuaries. *In*: Hydrodynamics of Estuaries and Fjords, J.C.J. Nihoul [Ed.], Elsevier Oceanography Series, *23*, pp. 261-281. Elsevier Scientific Publishing Company, Amsterdam.

Jamart, B.M., and D.F. Winter, 1980. Finite element computation of the barotropic tides in Knight Inlet, British Columbia. *In*: Fjord Oceanography, H.J. Freeland, D.M. Farmer, and C.D. Levings [Eds.], pp. 283-289, Plenum Publishing Corp., New York.

Kawahara, M., K. Hasegawa, and Y. Kawanago, 1977. Periodic tidal flow analysis by finite element perturbation method. Computers and Fluids, *5*(4): 175-189.

Kawahara, M., and K. Hasegawa, 1978. Periodic Galerkin finite element method of tidal flow. International Journal for Numerical Methods in Engineering, *12*: 115-127.

King, I.P., W.R. Norton, and K.R. Iceman, 1975. A finite element solution for two-dimensional stratified flow problems. *In:* Finite Elements in Fluids, Vol. 1, R.H. Gallagher, J.T. Oden, C. Taylor, and O.C. Zienkiewicz [Eds.], pp. 133-156. Wiley-Interscience, London.

LeBlond, P.H., and L.A. Mysak, 1978. Waves in the Ocean. Elsevier Oceanography Series, *20*, Elsevier Scientific Publishing Company, Amsterdam, 602 pp.

Lee, J.J., 1971. Wave-induced oscillations in harbours of arbitrary geometry. Journal of Fluid Mechanics, *45*(2): 375-394.

Leendertse, J.J., 1967. Aspects of a computational model for long-period water-wave propagation. Memorandum RM-5294-PR, The Rand Corporation, Santa Monica, California, 165 pp.

LeProvost, C., and A. Poncet, 1978. Finite element method for spectral modelling of tides. International Journal for Numerical Methods in Engineering, *12*: 853-871.

Lynch, D.R., 1978. Finite-element solution of the shallow water equations. Ph.D. dissertation, Princeton University, Princeton, New Jersey.

Maier-Reimer, E., 1977. Residual circulation in the North Sea due to the M_2-tide and mean annual wind stress. Deutsche Hydrographische Zeitschrift, Jahrgang *30*: 69-80.

Maxworthy, T., 1979. A note on the internal solitary waves produced by tidal flow over a three-dimensional ridge. Journal of Geophysical Research, *84*(C1): 338-346.

MIT/Marine Industry Collegium, 1977. Computer models for environmental engineering and research in near-coastal environments. Report No. MITSG 77-16, Massachusetts Institute of Technology, Cambridge, Massachusetts, 31 pp.

Pearson, C.E., 1977. Note on Kelvin wave reflection in a channel with an arbitrary end wall. Geophysical and Astrophysical Fluid Dynamics, *8*: 303-309.

Pearson, C.E., and D.F. Winter, 1977. On the calculation of tidal currents in homogeneous estuaries. Journal of Physical Oceanography, *7*(4): 520-531.

Pickard, G.L., 1956. Physical features of British Columbia inlets. Transactions of the Royal Society of Canada, *50*(3): 47-58.

Pickard, G.L, 1961. Oceanographic features of inlets in the British Columbia coast. Journal of the Fisheries Research Board of Canada, *18*(6): 907-999.

Pickard, G.L., and K. Rodgers, 1959. Current measurements in Knight Inlet, British Columbia. Journal of the Fisheries Research Board of Canada, *16*(5): 635-678.

Ramming, H.-G., 1976. A nested North Sea model with fine resolution in shallow coastal areas. Mémoires de la Société Royale des Sciences de Liège, 6ème Série, tome X: 9-26.

Ronday, F.C., 1976. Modèles hydrodynamiques. Projet Mer, Rapport Final. Services du Premier Ministre, Programmation de la Politique Scientifique, Bruxelles, Belgique.

Ronday, F.C., 1979. Tidal and residual circulations in the English Channel. *In*: Marine Forecasting, J.C.J. Nihoul [Ed.], Elsevier Oceanography Series, *25*, pp. 351-384. Elsevier Scientific Publishing Company, Amsterdam.

Schönfeld, J.C., 1951. Propagation of tides and similar waves. Ph.D. dissertation, Staatsdrukkerij en Uitgeverijbedrijf, 'S-Gravenhage, 232 pp.

Shi, N.C., 1978. A study of the nearshore current observations in Hood Canal, Washington. Masters of Science Thesis, University of Washington, Seattle, Washington, 96 pp.

Smith, J.D., and D.M. Farmer, 1977. Nonlinear internal waves and internal hydraulic jumps in a fjord. Geofluiddynamical waves mathematics: Research Contributions, Applied Mathematics Group, University of Washington, Seattle, Washington, pp. 42-53.

Snyder, R.L., M. Sidjabat, and J.H. Filloux, 1979. A study of tides, setup and bottom friction in a shallow semi-enclosed basin. Part II: Tidal model and comparison with data. Journal of Physical Oceanography, *9*(1): 170-188.

Swakon, Jr., E.A., and J.D. Wang, 1977. Modeling of tide and wind induced flow in South Biscayne Bay and Card Sound. University of Miami Sea Grant Technical Bulletin No. 37, 143 pp.

Taylor, G.I., 1919. Tidal friction in the Irish Sea. Philosophical Transactions of the Royal Society, A, *220*: 1-39.

Taylor, G.I., 1921. Tidal oscillations in gulfs and rectangular basins. Proceedings of the London Mathematical Society, *20*: 148-181.

Taylor, C., and J.M. Davis, 1975. Tidal propagation and dispersion in estuaries. *In*: Finite Elements in Fluids, Vol. 1, R.H. Gallagher, J.T. Oden, C. Taylor, and O.C. Zienkiewicz [Eds.], pp. 95-118. Wiley-Interscience, London.

Thomson, R.E., 1976. Tidal currents and estuarine-type circulation in Johnstone Strait, British Columbia. Journal of the Fisheries Research Board of Canada, *33*: 2242-2264.

Thomson, R.E., 1977. Currents in Johnstone Strait, British Columbia: supplemental data on the Vancouver Island side. Journal of the Fisheries Research Board of Canada, *34*: 697-703.

Walters, R.A., and R.T. Cheng, 1978. A two-dimensional hydrodynamic model of a tidal estuary. *In*: Finite Elements in Water Resources, C.A. Brebbia, W.G. Gray, and G.F. Pinder [Eds.], pp. 2.3-2.21. Pentech Press, London.

Wang, J.D., and J.J. Connor, 1975. Mathematical modeling of near coastal circulation. Report No. MITSG 75-13, Massachusetts Institute of Technology, Cambridge, Massachusetts, 272 pp.

Whalin, R.W., F.C. Perry, and D.L. Durham, 1976. Model verification for tidal constituents. *In*: Proceedings of the Fifteenth Coastal Engineering Conference, pp. 3377-3395. American Society of Civil Engineers, New York.